REPORT DOCUMENTATION PAGE

Form Approved
OMB No. 0704-0188

PLEASE DO NOT RETURN YOUR FORM TO THE ABOVE ORGANIZATION.

1. REPORT DATE *(DD-MM-YYYY)*	2. REPORT TYPE	3. DATES COVERED *(From - To)*
8SEPT 2009	Final	15AUG 2002 to 14AUG 2008

4. TITLE AND SUBTITLE
(DARPA) MICRORESCONATOR AND PHOTONIC CRYSTAL FILTERS, LASERS AND MODULATORS FOR ANALOG AND DIGITAL CHIP SCALE WDM SYSTEMS

5a. CONTRACT NUMBER

5b. GRANT NUMBER
F49620-02-1-0403

5c. PROGRAM ELEMENT NUMBER

6. AUTHOR(S)
JOHN O'BRIEN
UNIV OF SOUTHERN CALIFORNIA
ELECTRICAL ENGINEERING-ELECTROPHYISCS

5d. PROJECT NUMBER

5e. TASK NUMBER

5f. WORK UNIT NUMBER

7. PERFORMING ORGANIZATION NAME(S) AND ADDRESS(ES)
GAYLE LUND, CONTRACTS & GRANTS
UNIV OF SOUTHERN CALIFORNIA
837 DOWNEY WAY, STO 330, LOS ANGELES, CA 90089-0271

8. PERFORMING ORGANIZATION REPORT NUMBER

9. SPONSORING/MONITORING AGENCY NAME(S) AND ADDRESS(ES)
AF OFFICE OF SCIENTIFIC RESEARCH
875 NORTH RANDOLPH STREET ROOM 3112
ARLINGTON VA 22203

10. SPONSOR/MONITOR'S ACRONYM(S)

11. SPONSOR/MONITOR'S REPORT NUMBER(S)
AFRL-OSR-VA-TR-2012-0101

12. DISTRIBUTION/AVAILABILITY STATEMENT
UNLIMITED

13. SUPPLEMENTARY NOTES

14. ABSTRACT
Networks play an important role in the overall functioning of military weapons systems, and WDM (wavelength division multiplexing) technology offers many potentially substantial improvements to the performance of these networks as well as to the host platform. Future military platforms would see substantial benefit from WDM components that provide high levels of chip-scale integration, support dynamically reconfigurable topologies, offer data format independence (support different digital data types as well as the ability to simultaneously transport digital and analog data), and are temperature robust. The outcome of this specific research will develop highly integrateable functional components that will enable the fabrication of chip-scale WDM signal-processing systems. This will provide secure, compact, low-power, high-bandwidth systems.

15. SUBJECT TERMS

16. SECURITY CLASSIFICATION OF:			17. LIMITATION OF ABSTRACT	18. NUMBER OF PAGES	19a. NAME OF RESPONSIBLE PERSON
a. REPORT	b. ABSTRACT	c. THIS PAGE			JOHN O'BRIEN
					19b. TELEPHONE NUMBER *(Include area code)* 213-740-8682

USC
UNIVERSITY
OF SOUTHERN
CALIFORNIA

September 8, 2009

Department of
Contracts and Grants

AFOSR
Attn: Gavin Arora
875 N. Randolph Street
Suite 325, Room3112
Arlington, VA 22203-1768

Subject: Grant No.: F49620-02-1-0403
Final Technical Report

On behalf of the University, enclosed is a copy of the subject document, which has been submitted to AFOSR on 09/04/2009 by Principal Investigator, Dr. John O'Brien.

Please feel free to call me at (213) 740-2875 if you have any questions.

Sincerely,

Melaina Trotter
Closeout Specialist

cc: Beth Swing – ONR, San Diego
USC Account No.: 53-4502-1360

University of
Southern California
Los Angeles,
California 90089-1147
Tel: 213 740 7762
Fax: 213 740 6070
web page:
www.usc.edu/dept/
contracts/

Microresonator and Photonic Crystal Filters, Lasers, and Modulators for Analog and Digital Chip Scale WDM Systems (CSWDM)

Microresonator Final Report

John D. O'Brien

P. Daniel Dapkus

Contents

CSWDM Microresonator Publications

1. Choi SJ, Lin W, Djordjev K, Choi SJ, Dapkus PD, Griffel G, Menna R, Connolly J. *Microring resonators vertically coupled to buried heterostructure bus waveguides.* Integrated Photonics Research (Trends in Optics and Photonics Series Vol.91); 2003; USA. Optical Soc. of America. p 151-4. (Integrated Photonics Research (Trends in Optics and Photonics Series Vol.91)).
2. Choi SJ, Peng Z, Yang Q, Choi SJ, Dapkus PD. *8-channel microdisk CW laser arrays vertically coupled to low-loss common bus waveguides.* 2003 IEEE LEOS Annual Meeting Conference Proceedings (IEEE Cat. No.03CH37460); 2003; Tucson, AZ, USA. IEEE. p 822-3. (2003 IEEE LEOS Annual Meeting Conference Proceedings (IEEE Cat. No.03CH37460)).
3. Choi SJ, Zhen P, Qi Y, Sang Jun C, Dapkus PD. *8-channel tunable MUX/DEMUX using vertically coupled active microdisk resonators.* 2003 IEEE LEOS Annual Meeting Conference Proceedings (IEEE Cat. No.03CH37460); 2003; Tucson, AZ, USA. IEEE. p 287-8. (2003 IEEE LEOS Annual Meeting Conference Proceedings (IEEE Cat. No.03CH37460)).
4. Dapkus PD, O'Brien JD. *Meso- and nanophotonic devices for integrated photonic circuits.* 61st Device Research Conference. Conference Digest (Cat. No.03TH8663); 2003; Salt Lake City, UT, USA. IEEE. p 121. (61st Device Research Conference. Conference Digest (Cat. No.03TH8663)).
5. Seung June C, Djordjev K, Sang Jun C, Dapkus PD. *Microdisk lasers vertically coupled to output waveguides.* IEEE Photonics Technology Letters 2003;15(10):1330-2.
6. Yang Q, Choi J, Djordjev K, Choi SJ, Dapkus PD. *Realization of a high-contrast optical filter by a semiconductor double-disk resonator.* Integrated Photonics Research (Trends in Optics and Photonics Series Vol.91); 2003; USA. Optical Soc. of America. p 155-8. (Integrated Photonics Research (Trends in Optics and Photonics Series Vol.91)).
7. Choi SJ, Djordjev K, Sang Jun C, Dapkus PD, Lin W, Griffel G, Menna R, Connolly J. *Microring resonators vertically coupled to buried heterostructure bus waveguides.* IEEE Photonics Technology Letters 2004;16(3):828-30.
8. Choi SJ, Djordjev K, Zhen P, Qi Y, Sang Jun C, Dapkus PD. *Laterally coupled buried heterostructure high-Q ring resonators.* IEEE Photonics Technology Letters 2004;16(10):2266-8.
9. Choi SJ, Zhen P, Qi Y, Sang Jun C, Dapkus PD. *Tunable microdisk resonators vertically coupled to bus waveguides using epitaxial regrowth and wafer bonding techniques.* Applied Physics Letters 2004;84(5):651-3.
10. Choi SJ, Zhen P, Qi Y, Sang Jun C, Dapkus PD. *An eight-channel demultiplexing switch array using vertically coupled active semiconductor microdisk resonators.* IEEE Photonics Technology Letters 2004;16(11):2517-19.
11. Dapkus PD, Seung June C, Qi Y, Zhen P, Sadagopan T, Sang Jun C. *Technology for active photonic integrated circuits-based on semiconductor microresonators.* 2004 IEEE LEOS Annual Meeting Conference Proceedings (IEEE Cat. No.04CH37581); 2004; Rio Grande, Puerto Rico. IEEE. p 358-9. (2004 IEEE LEOS Annual Meeting Conference Proceedings (IEEE Cat. No.04CH37581)).
12. Jang JW, Pyun SH, Lee SH, Lee IC, Jeong WG, Stevenson R, Dapkus PD, Kim NJ, Hwang MS, Lee D. *Room temperature operation of InGaAs/InGaAsP/InP quantum dot lasers.* Applied Physics Letters 2004;85(17):3675-7.

13. Khatsevich S, Rich DH, Zhang X, Zhou W, Dapkus PD. *Temperature dependence of excitonic recombination in lateral epitaxially overgrown InGaN/GaN quantum wells studied with cathodoluminescence.* Journal of Applied Physics 2004;95(4):1832-42.
14. Pataro LL, Yuanming D, Dapkus PD. *Asymmetric heterostructure design considerations for high-power laser.* 2004 IEEE LEOS Annual Meeting Conference Proceedings (IEEE Cat. No.04CH37581); 2004; Rio Grande, Puerto Rico. IEEE. p 469-70. (2004 IEEE LEOS Annual Meeting Conference Proceedings (IEEE Cat. No.04CH37581)).
15. Pyun SH, Lee SH, Lee IC, Jeong WG, Jang JW, Stevenson R, Dapkus PD, Lee D, Lee JH, Oh DK. *Room temperature cw operation of InGaAs/InGaAsP/InP quantum dot lasers.* Conference Digest. 2004 IEEE 19th International Semiconductor Laser Conference (IEEE Cat. No.04CH37594); 2004; Matsue-shi, Japan. IEEE. p 59-60. (Conference Digest. 2004 IEEE 19th International Semiconductor Laser Conference (IEEE Cat. No.04CH37594)).
16. Sadagopan T, Seung June C, Sang Jun C, Dapkus PD, Bond A. *High-speed, low-voltage modulation in circular WGM microresonators.* 2004 Digest of the LEOS Summer Topical Meetings: Biophotonics/Optical Interconnects & VLSI Photonics/WGM Microcavities (IEEE Cat. No.04TH8728); 2004; San Diego, CA, USA. IEEE. p 2 pp. (2004 Digest of the LEOS Summer Topical Meetings: Biophotonics/Optical Interconnects & VLSI Photonics/WGM Microcavities (IEEE Cat. No.04TH8728)).
17. Seung June C, Qi Y, Zhen P, Sang Jun C, Dapkus PD. *High-Q buried heterostructure microring resonators.* Conference on Lasers and Electro-Optics (CLEO); 2004; San Francisco, CA, USA. IEEE. p 3 pp. vol.2. (Conference on Lasers and Electro-Optics (CLEO)).
18. Seung June C, Zhen P, Qi Y, Sang Jun C, Dapkus PD. *All-buried active microring resonators using vernier effects for free spectral range expansion and optical channel configuration.* 2004 Digest of the LEOS Summer Topical Meetings: Biophotonics/Optical Interconnects & VLSI Photonics/WGM Microcavities (IEEE Cat. No.04TH8728); 2004; San Diego, CA, USA. IEEE. p 2 pp. (2004 Digest of the LEOS Summer Topical Meetings: Biophotonics/Optical Interconnects & VLSI Photonics/WGM Microcavities (IEEE Cat. No.04TH8728)).
19. Seung June C, Zhen P, Qi Y, Sang Jun C, Dapkus PD. *Eight-channel microdisk CW laser arrays vertically coupled to common output bus waveguides.* IEEE Photonics Technology Letters 2004;16(2):356-8.
20. Choi SJ, Zhen P, Qi Y, Eui Hyun H, Dapkus PD. *A high-Q wavelength filter based on buried heterostructure ring resonators integrated with a semiconductor optical amplifier.* IEEE Photonics Technology Letters 2005;17(10):2101-3.
21. Choi SJ, Zhen P, Qi Y, Sang Jun C, Dapkus PD. *Bus-coupled microresonator lasers.* Proc. SPIE - Int. Soc. Opt. Eng. (USA); 2005; San Jose, CA, USA. SPIE-Int. Soc. Opt. Eng. p 285-94. (Proc. SPIE - Int. Soc. Opt. Eng. (USA)).
22. Choi SJ, Zhen P, Qi Y, Sang Jun C, Dapkus PD. *Tunable narrow linewidth all-buried heterostructure ring resonator filters using vernier effects.* IEEE Photonics Technology Letters 2005;17(1):106-8.
23. June S, Choi, Dapkus PD, Yang Q, Peng Z, Choi SJ, Hwang EH. *High-Q buried heterostructure resonators for photonic integrated circuits.* 2005 Conference on Lasers and Electro-Optics (CLEO) (IEEE Cat. No. 05TH8796); 2005; Baltimore, MD, USA. IEEE. p 553-5. (2005 Conference on Lasers and Electro-Optics (CLEO) (IEEE Cat. No. 05TH8796)).

24. Kim HD, Jeong WG, Jang JW, Pyun SH, Hwang MS, Lee D, Stevenson R, Dapkus PD. *1.5 μm InGaAs/InGaAsP/InP quantum dot lasers operating CW at room temperature.* 2005 Optical Fiber Communications Conference Technical Digest (IEEE Cat. No. 05CH37672); 2005; Anaheim, CA, USA. IEEE. p 3 pp. Vol. 3. (2005 Optical Fiber Communications Conference Technical Digest (IEEE Cat. No. 05CH37672)).
25. Kim HD, Jeong WG, Lee JH, Yim JS, Lee D, Stevenson R, Dapkus PD, Jang JW, Pyun SH. Continuous-wave operation of 1.5 μm InGaAs/InGaAsP/InP quantum dot lasers at room temperature. Applied Physics Letters 2005;87(8):83110-1.
26. Ren D, Wei Z, Dapkus PD. *Low-dislocation-density, nonplanar GaN templates for buried heterostructure lasers grown by lateral epitaxial overgrowth*. Applied Physics Letters 2005;86(11):111901-1.
27. Sadagopan T, Choi SJ, Sang Jun C, Dapkus PD, Bond AE. Optical Modulators based on depletion width translation in semiconductor microdisk resonators. IEEE Photonics Technology Letters 2005;17(3):567-9.
28. Sadagopan T, Choi SJ, Sang Jun C, Djordjev K, Dapkus PD. *Carrier-induced refractive index changes in InP-based circular microresonators for low-voltage high-speed modulation.* IEEE Photonics Technology Letters 2005;17(2):414-16.
29. Seung June C, Zhen P, Qi Y, Eui Hyun H, Dapkus PD. *A semiconductor tunable laser using a wavelength selective reflector based on ring resonators.* 2005 Optical Fiber Communications Conference Post deadline Papers (IEEE Cat. No. 05CH37672); 2005; Anaheim, CA, USA. IEEE. p 3 pp. Vol. 5. (2005 Optical Fiber Communications Conference Post deadline Papers (IEEE Cat. No. 05CH37672)).

Semiconductor Microresonators - Introduction

The part of USC's CSWDM program involving semiconductor microresonators had the goal to demonstrate useful functionality of InP mIcroresonators for application in military photonic systems. microresonators are highly functional optical device elements that can be used in many different roles within a photonic integrated system. As a passive element they can be used as narrow band filters that that can be cascaded to affect the shape of the pass band and as active devices are tunable and switchable. This functionality can be used as a digital or analog filter, a space switch, or a modulator depending on the tuning speed. When gain is incorporated into the active region of the resonator, they can be operated as lossless filters or as lasers. Since multiple resonators with different resonances can in principle be coupled to the same waveguide the array of devices can serve and multiplexers and demultiplexers, laser arrays or modulator arrays for a manifold of WDM wavelengths. The basic building block of the work is a circular microresonator vertically coupled to a waveguide as shown in the figure below. The disk layers and the waveguide layers are grown from a single epitaxial run with the waveguide layers grown on top. The waveguides are defined by dry etching and the layer structure is bonded to another InP wafer after which the original growth substrate is removed. The resonator is then defined and etched and contacts are applied if desired.

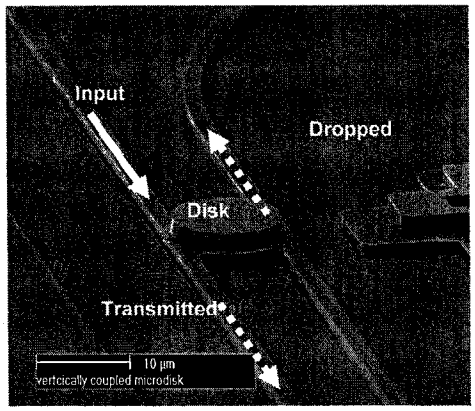

Single element MR coupler.

These resonators have typical Q's in the range of 10,000 and are tunable over 2-3 nm by the application of a forward bias that injects carriers into the resonator waveguide region. This approach results in a maximum tuning / modulation speed of 500 MHz. Designs were also explored that employed carrier extraction by a reverse bias to achieve rapid capacitance limited tuning at a speed of 10 GHz.

During the course of the program other technology approaches were developed. In one the waveguides were fabricated as buried heterostructures and the resonator layer was grown on top. This approach was attempted to increased the current uniformity in the resonator but had the deleterious effect that the losses in the resonator were increased owing to light leakage into the substrate.

We also developed an all buried laterally coupled resonator structure with very high Q that was incorporated into a Vernier tuned resonator with very wide tuning range. This will be discussed later.

A set of aggressive milestones were set for the program t enable one to test the viability of the technology for military applications. Those milestones are listed below:

- ✓ Demonstrate 4 element arrays of tunable resonators separated by 1.6 nm within the $C_{\square}$ band that are tunable by free carrier injection over >2 nm with a linewidth < 0.3 nm over the entire tuning range with tuning / switching speed, f_{switch} =1 MHz.(Q4)
- ✓ Demonstrate four element arrays of single frequency lasers with resonator stabilization. Element wavelength separation > 2nm, modulation rate = 1Gb/s. (Q4)
- ✓ Demonstrate actively tuned multipole resonator circuit with > 2 nm tuning range and > 30 dB suppression of adjacent resonances separated by 1.6 nm. (Q8)

- Demonstrate resonator circuit to actively control transfer function over temperature range of 0 – 70 C.(Q10)
- Demonstrate compact, temperature stable (0 – 70 C) 8 ? MUX/DEMUX with 0.8 nm channel separation and >-30 dB crosstalk . (Q12)
- ✓ Demonstrate tunable (20 nm) resonator based laser in C? band. (Q12)
- ✓ Demonstrate widely tunable (>30 nm) dual resonator laser over entire C? band.(Q16)
- Demonstrate polarization insensitive 8 ? DEMUX. (Q16)

The milestones with check marks were met during the program.

Microresonator Lasers and Multiplexers

During the first year of the program, USC investigated the issues involved in the fabrication of semiconductor laser arrays and multiplexers/demultiplexers (MUX/DEMUX) using arrays of microresonators (MR) coupled to waveguides. Prior to the start of the program, we had demonstrated single element MR lasers and MR waveguide couplers using vertically coupled elements. Examples of the single element devices are shown in the figures below.

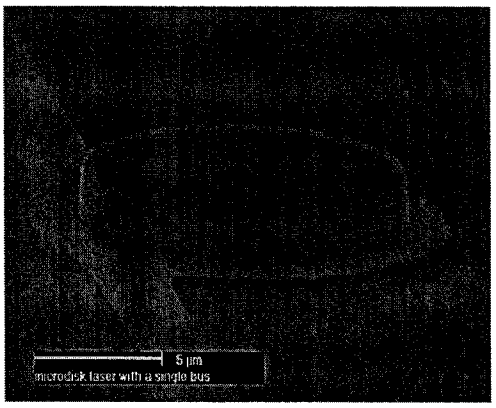

Single element MR laser vertically coupled to a waveguide

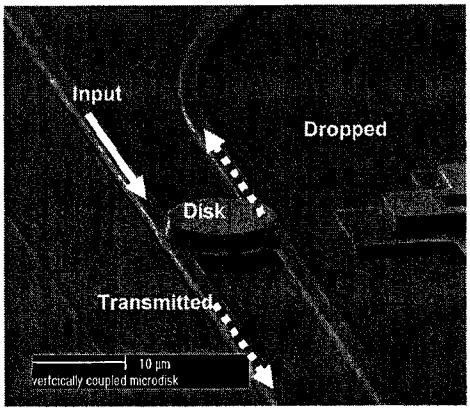

Single element MR coupler.

The devices are shown without metallization to illustrate the physical structures. Prior to the start of the program the lasers were operated CW but exhibited very pronounced kinks in the light output versus current characteristics resulting from mode competition. The cause of the kinking was determined to be thermal tuning of the laser that caused mode hopping between closely spaced azimuthal modes. One objective of the program is to correct this thermal tuning by creating a thermally more-stable structure, to demonstrate single mode operation and to demonstrate eight element arrays of lasers.

The MUX/DEMUX is to be based on the coupler illustrated in figure 4. The transfer characteristic of this

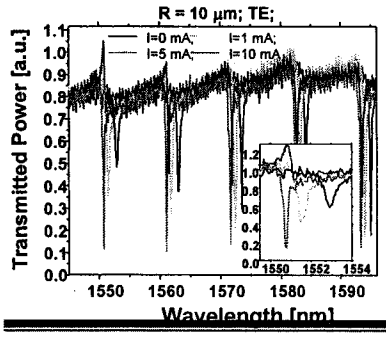

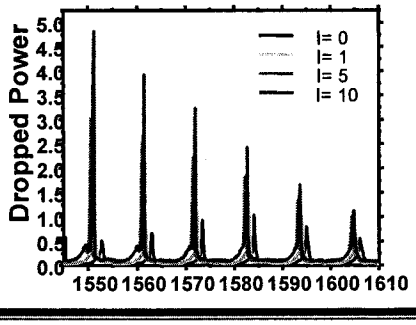

(left) Transmitted spectrum from through port and (right) dropped port spectrum showing resonances in single resonator coupler and the effects of forward current drive in the resonator and resonance wavelength and gain near the band edge.

device is shown in the figures below. Here we show the transmission and drop port characteristics of a device whose index of refraction and loss are tuned by the injection of free carriers into the disk. The change in index at wavelengths longer than the bandgap (~1.55 μm) causes a blue shift of the resonance peaks in both ports. Near and above the band edge, this shift is accompanied by a change in the loss characteristics owing to the creation of gain above the band gap. The high Q of the resonators is illustrated by the narrow resonance characteristics. Our objective in this program is to use those structures to fabricate an eight wavelength MUX/DEMUX.

Single Mode Laser

In this section, we present low threshold, single mode continuous-wave (CW) operation of microdisk resonator lasers that are vertically coupled to bus waveguides. Vertically coupled epitaxial structures afford the freedom in choosing independent material composition for disks and waveguides and provide the precise control of coupling coefficient. More over, vertically coupled microdisk lasers utilize technologies entirely compatible with approaches for fabricating passive and active microdisks [1-3], which makes it feasible to realize monolithic PIC's. By using a single design for the active region, various types of PIC elements, such as optical switches utilizing electroabsorption [2] and gain [3], can be produced along with the microdisk lasers on a wafer.

The epitaxial wafer structure used for the vertically coupled microdisk lasers has two vertically stacked waveguides, the I/O bus waveguide and the active (QW) disk core, respectively, that are separated by an 800-nm thick InP coupling layer. The disk core, with total thickness of 400 nm, consists of two separate confinement layers (SCH) with λ_{SCH} = 1250 nm, 4 QW's (1% compressively-strained) with emission wavelength at λ_W = 1575 nm, and 3 barriers with λ_B = 1250 nm. Next, the n-doped InP coupling layer and the n-doped I/O bus waveguide layer (thickness?) with λ_{WG} = 1100 nm are grown followed by the top n-cladding InP layers.

To initiate the device definition, I/O bus waveguides are lithographically defined and dry etched, and the entire structure is flipped over and thermally bonded to another InP transfer wafer. Then, the wafer-bonded sample is mechanically polished and the remaining InP from the original substrate is completely removed by selective chemical wet etching solutions to provide access to the disk waveguide structure for further patterning. Very smooth and vertical microdisk mesas were formed on the exposed surface by using $CH_4/H_2/Ar$ chemistry in a reactive ion etching (RIE) discharge [4]. Figure 1 shows an SEM image of vertically coupled microdisk devices that were taken after the disk formation. A 0.7-μm-wide single mode bus waveguide is used with the microdisk to out-couple the lasing WGM. The device has a post under the microdisk, separated from the bus waveguide by ~ 1 □m, serving as the current path to ground. Details on further fabrication processes, including surface planarization and metal contacts, can be found in references [1-3]. The wafer is thinned and bars are cleaved 600 μm long for the measurement. Anti reflection (AR) coating is deposited on both facets to suppress undesired Fabry-Perot resonance from the bus waveguides.

We observed CW lasing at room temperature for 8- and 10-μm-radii microdisk resonators. Effective mode indices (n_{eff}) of 3.115 and 3.145 are calculated for 8- and 10-μm-radii disks, respectively, to identify the mode numbers. The power-coupling coefficient (κ) between the disk cavity and the vertically coupled bus waveguide was estimated by measuring the quality factor (Q) and the transmission characteristics of microdisk resonators as passive structures coupled to the bus. Using the measured Q value (5000~6000), κ = 4~5 % is obtained for the present devices [1-3].

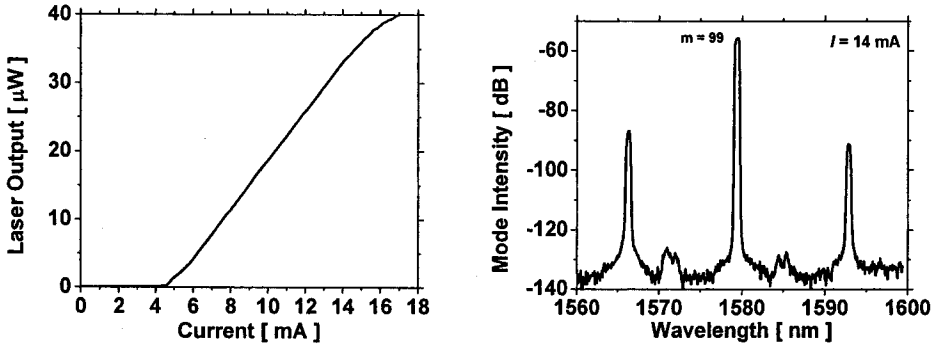

(left) L-I characteristics of single mode MR laser. (right) Spectrum of single mode MR laser.

The measured *L-I* curve for an 8-μm-radius microdisk laser is shown in Fig. (a), where low threshold (I_{TH} = 4.5 mA), single mode CW operation is achieved. Figure 5 (b) shows the lasing spectrum measured at I = 14 mA. The amplified spontaneous emission in the active region is coupled into the disk WGM modes resulting in periodic peaks in the output spectra. A FSR of 13 nm is obtained from 8-μm-radii disks. The large FSR results in less number of optical modes in the spectral range of interest, which makes it more probable to have a single mode operation. Computer-aided calculation indicates that the wavelength for maximum gain density is placed at $\lambda_{Max\text{-}Gain}$ = 1580 nm. A single lasing mode centered at 1579 nm is obtained for an 8-μm-radius disk with a large side mode suppression ratio of 30 dB over a pumping range > 3X threshold. The detuning of the lasing wavelength resulting from blue shifts due to the carrier injection and band filling effects at moderate forward currents and red shifts caused by thermal effects at higher injection, respectively, is within ±0.5 nm for I = 4.5~17 mA.

For larger disks, on the other hand, single mode operation under CW conditions was not obtainable at room temperature. Figure 5 shows the measured lasing spectra for a 10-μm-radius disk at different

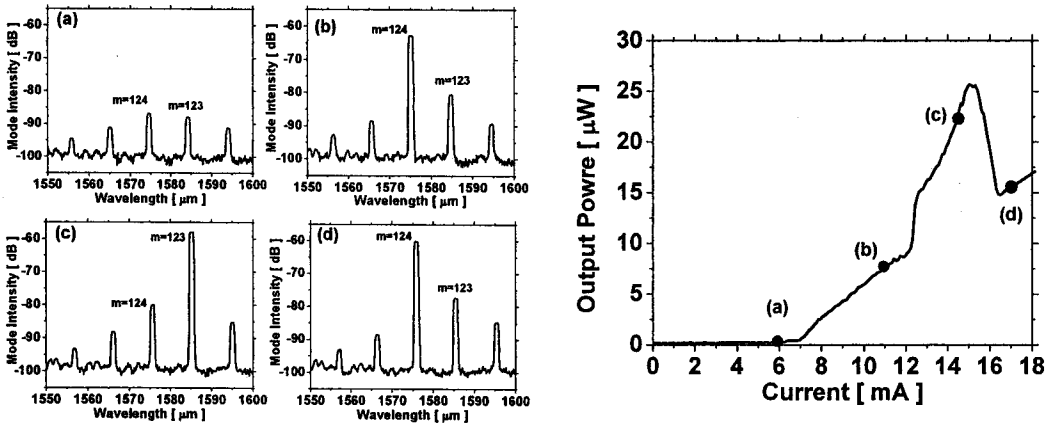

(left) Spectra of MR laser under different operating conditions illustrating mode hopping.
(right) L-I characteristics of same laser showing pronounced kinks in characteristics resulting from mode hopping

current levels. The 10-μm-radius disk has a smaller FSR of 9.5 nm. As forward current increases, m = ±124 mode at 1574.5 nm acquires sufficient gain to begin lasing, followed by m = ±123 mode at 1584 nm at higher currents. It is observed that the peak intensities of two adjacent modes, m = ±125 at 1574.5 nm and m = ±124 at 1584 nm, oscillate over a range of currents. Both of the oscillating modes are placed very close to $\lambda_{Max\text{-}Gain}$ and are readily involved in a gain competition process. Since the gain spectrum is highly sensitive to temperature and carrier concentration in the active region, non-uniform heat and

current distributions inside the disk cavity may cause the lasing mode to 'hop' as seen above. The mode hopping leads to abrupt 'kinks' in the measured *L-I* characteristics as shown. Similar results have been observed from 12-μm-radii disks. To avoid mode competition, adjacent modes must be separated by larger FSR, which can be achieved by reducing the disk size.

InP/InGaAsP microdisk resonator lasers are demonstrated, where high-*Q* disk modes are coupled out through the vertically coupled straight bus waveguides. The suggested structures are considered to meet the demand for a light source in PIC's, due to the freedom in designing a low-loss common bus line and the use of fabrication technologies comaptible with integration of other PIC elements. Under CW operation, a single mode laser with an SMSR greater than 30 dB has been achieved for an 8-μm-radius microdisk. For larger disks, mode competition between modes near the maximum gain density wavelength is observed from the *L-I* characteristics. Future devices will be designed with smaller radius to reduce the mode competition and with ring geometry to reduce the operating current and improve the heat sink capability.

[1] K. D. Djordjev S. J. Choi, S. J. Choi, and P. D. Dapkus, "Active semiconductor microdisk devices", *IEEE J. Light. Technol.*, vol.20, pp. 105-113, Jan. 2002.
[2] K. D. Djordjev S. J. Choi, S. J. Choi, and P. D. Dapkus, "Vertically coupled InP microdisk switching devices with electroabsorptive active regions", *IEEE Photon. Technol. Lett.*, vol.14, pp. 1115-1117, Aug. 2002.
[3] K. D. Djordjev, S. J. Choi, S. J. Choi, and P. D. Dapkus, "Gain trimming of the resonant characteristics in vertically coupled InP microdisk Switches", *Appl. Phys. Lett.*, vol. 80, pp. 3467-3469, May 2002.
[4] S. J. Choi, K. D. Djordjev, S. J. Choi, and P. D. Dapkus, "CH4-based dry etching of high Q InP microdisks", *J. Vac. Sci. Technol. B*, vol. 20, pp. 301-305, Jan. 2002.

Eight channel microresonator laser array with 1.6 nm channel spacing coupled to a common output waveguide.

In this section, we present 8-channel continuous-wave (CW) laser arrays using vertically coupled microdisk resonators. The microdisks have slightly different radii and offer 1.6 nm spectral channel spacing that corresponds to the 200 GHz international telecommunications union (ITU) grid spacing in optical wavelength division multiplexing (WDM) protocols. These lasers utilize technologies entirely compatible with the approaches for fabricating tunable filters and switches [1-3], which makes it feasible to realize monolithic PIC's.

The epitaxial wafer structure used for the vertically coupled microdisk lasers has two vertically stacked waveguides, the I/O bus waveguide and the active (QW) disk core, respectively, that are separated by a 0.8-μm thick InP coupling layer. The disk core, with total thickness of 0.4μm, consists of two separate confinement layers (SCH) with λ_{SCH} = 1.25 μm and 4 QW's (0.5% compressively-strained) with emission wavelength at λ_w= 1.51 μm and 3 barriers with λ_b = 1.25 μm. Next, the n-doped coupling layer and the n-doped (~ 3×10^{17} cm^{-3}) I/O bus waveguide layer with λ_{WG} = 1.1 μm are grown followed by the top n-cladding InP layers.

To initiate the device fabrication, I/O bus waveguides are lithographically defined and dry etched. The entire structure is then flipped over and thermally bonded to another InP transfer wafer. The wafer-bonded sample is polished and the remaining InP from the original substrate is completely removed by selective chemical wet etching solutions. Smooth microdisk mesas with vertical sidewalls are produced on the exposed surface by using CH_4-based chemistry in an RIE discharge [4]. The disk radii (*r*) vary from 10.6 to 10.95 μm with 0.05 μm difference on average to achieve 1.6 nm spectral spacing for 8 channels. After the device surface is planarized by photosensitive polyimide, electrodes are formed on the disks. Cured polyimide patterns serve as self-aligned openings for the metal contacts that afford efficient current injection into the disks along the periphery region. The low heat conductivity (typically, 0.2 ~ 0.4

W/K·m) of polyimide ensures good thermal insulation between the disks so that biasing one laser does not affect the adjacent laser through heating effects. Details on further processes can be found in references [1-3]. A micrograph showing the top view of the fabricated disk array is given below. The 8-channel microdisk lasers are connected through a common output bus waveguide that is 480 μm long.

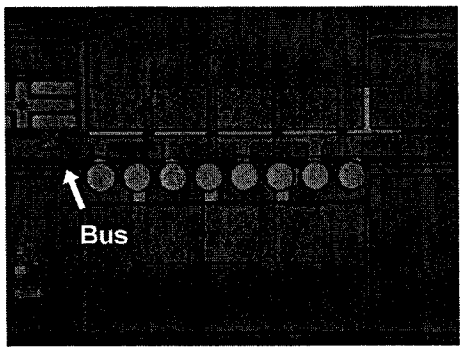

Micrograph of 8 channel MR laser array coupled to a single waveguide.

The suggested waveguide structure implies that the bus lines are n-type doped and have fairly high contrast index profiles in the lateral direction, which may cause free carrier induced absorption and scattering losses, respectively. The measured optical losses in the presented bus waveguides are 3 ~ 5 cm^{-1} [9]. The implementation of undoped, buried heterostructure (BH) bus waveguides will enable great reduction of the bus losses for future devices. [5-6].

Bus-coupled microdisk lasers can be modeled in a proximate manner as Fabry-Perot interferometers where the coupling junctions between the resonators and the buses form the mirrors. The reflectivity of the mirrors can be expressed by R_1 = 1- κ_1 and R_2 = 1- κ_2, where κ_1 (or κ_2) denotes the optical power coupling coefficient between the first (or the second) bus waveguide and the disk resonator. When the residual loss (α_i) and the traveling length (L) of a lasing cavity are known, the threshold gain (g_{th}) can be expressed as follows:

$$g_{th} = \alpha_i + \frac{1}{L}\ln(\frac{1}{R}), \text{where } L = \pi r \text{ and } R = \sqrt{R_1 R_2} \quad (1)$$

For the given device structures, α_i, r, κ_1 and κ_2 are found to be ~ 5 cm^{-1}, 10.6 ~ 10.95 μm, ~ 0.05 and 0 (i.e. the disk is coupled to a single bus line), respectively . The estimated threshold modal gain is $g_{th} \approx 20$ cm^{-1}. It is straightforward to see that g_{th} increases with κ. The κ must be maintained at moderate values not to have g_{th} exceed the maximum attainable gain for lasing. Ideally, the resonant wavelength is not to be affected by κ. However, in actual devices, the change in κ is usually achieved by altering the material and/or geometry of the disk resonators, which affects the modal index and the resultant lasing wavelength as well.

CW lasing at room temperature for an 8-channel microdisk array is measured. We use a free-space optical lens that is precisely aligned to one of the bus waveguides and collects the output laser coupled through the AR-coated bus facets. The typical output power measured from a single microdisk laser, which is spectrally integrated by a photo-detector, exceeds 20 μW at a pumping range of $I \approx 1.5 \times I_{th}$. The maximum output power is saturated at 40 μW or slightly higher for $I > 2.5 \times I_{th}$. Several abrupt 'kinks' appear in the measured *L-I* characteristics for certain devices, which results from mode hopping. When adjacent disk modes, having different radial distributions or azimuthal mode numbers, are not spectrally remote enough from one another and if both modes are comparably close to the peak gain spectrum, these modes are readily involved in a competition process to acquire gain that results in lasing mode hopping over a range of currents. To avoid mode oscillation, adjacent modes must be separated by larger free spectral range (FSR), which can be achieved by reducing the disk size. The large FSR results in fewer optical modes in the spectral range of interest, which makes it more probable to have single mode operation. Also, improved heat sinks are essential to stabilize the gain characteristics.

The resonant wavelength of a microdisk laser is determined by the resonant condition: $2\pi r n_{eff} = m \times \lambda_{resonant}$ (m is an integer), where n_{eff} is the effective modal index. For the given device geometries, Δr = 0.05 μm leads to $\Delta\lambda_{resonant}$ = 7.2 ~ 7.6 nm for the same azimuthal mode number m, in the spectral range of interest. Considering the typical FSR (~ 9 nm) of the presented resonators, we note that $\lambda_{resonant}(r, m)$

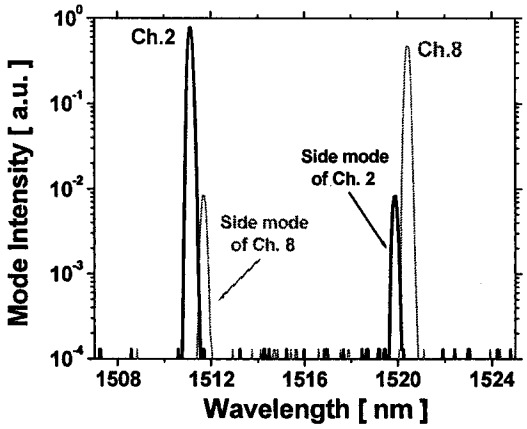

Fig. 9 Laser spectra of channels 2 and 8 showing overlap of spectra under laser operation when the lasers are multimode.

- $\lambda_{resonant}(r + \Delta r, m\text{-}1)$ = 1.4 ~ 1.8 nm. Therefore, by making slight variations in the disk radii ($r \rightarrow r + \Delta r$) and choosing the adjacent mode numbers ($m \rightarrow m$-1), we can achieve the desired spectral channel spacing of ~ 1.6 nm. As a matter of fact, $\lambda_{resonant}$ is highly sensitive to the physical dimension of resonators and the spectral spacing between channels is often detuned, due to probable fabrication errors. Slightly detuned characteristics can be corrected by adjusting the bias.

The lasing spectra are measured in the same manner as the *L-I* curves, but using a cleaved multi-mode optical fiber probed to a spectrum analyzer. The figure on the left shows the lasing spectra measured with a spectral resolution of 0.04 nm at I = 10 and 13 mA for channels 2 and 8, respectively. Since the amplified spontaneous emissions in the active region are coupled into the disk WGM's, periodic peaks are observed in the output spectra. The FSR of the given devices is ~ 9 nm, less than the bandwidth containing the entire 8 channels (1.6 nm × 7 = 11.2 nm), which means that certain side modes will exist in between the laser channels. For instance, the nearest side mode of channel 2 (1511.1 nm) appears close to the lasing spectrum of channel 8 (1520.4 nm) and vise versa. Those satellite modes may cause detrimental optical crosstalk unless they are distinctly separated from the actual lasing channels. We also observe that the lasing modes are clearly distinguished by very narrow linewidth of 0.25 nm and the side modes are effectively suppressed with high side mode suppression ratio (SMSR) of -20 dB.

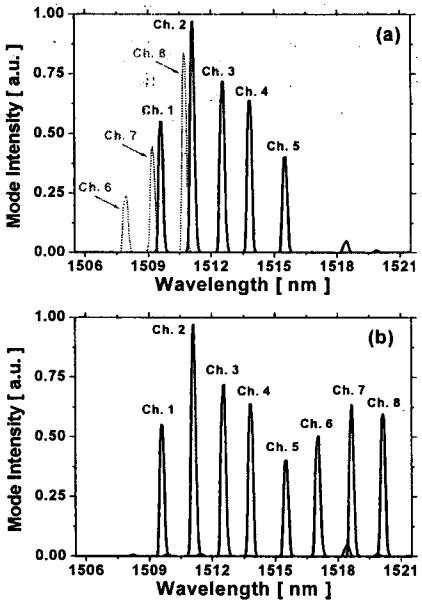

(a) shows the superimposed lasing spectra measured from 8 different microdisks in the laser array, where the microdisks are equally pumped at I = 10 mA. The resonant mode nearest to the peak gain spectrum will acquire enough optical gain for lasing in each channel, and the resultant peak intensity contour of the 8 channel lasing spectra resemble the original gain characteristics of the QW's centered at 1510 nm at low currents (over a pumping range < 1.5 × threshold) . However, at the given current injection level, the lasers wavelengths for channels 6, 7, and 8 are not achieved at the designed 1.6 nm channel spacing. The lasing modes for those channel can be corrected by red-shifting the gain and the spontaneous emission spectra the QW's. Higher injection levels are required to red-shift the effective QW bandedge by thermal effects. When I = 13 mA is applied for channels 6, 7, and 8, the lasing modes 'hop' to the next resonant modes at longer wavelengths and we successfully realize 1.6-nm-spectrally-spaced, 8-channel laser array as given in Fig.(b). As a matter of fact, we 'utilize' the mode hopping phenomena to obtain the desired channel spacing, which is not actually favorable for ideal laser arrays. This first demonstration of a compact laser

array using microresonators suggests the future direction for improved device performances. In ideal designs, the resonant modes of each microdisk must be separated by large FSR's so that each channel has only one optical mode placed within a gain spectral region.

In conclusion, 1.6-nm-spectrally-spaced, 8-channel CW laser arrays are achieved by integrating active microdisk resonators with a single bus waveguide. Typically, a measured linewidth of 0.25 nm and SMSR greater than 20 dB are observed for the microdisks lasing at near λ = 1.51 μm under CW operation. This is the first demonstration of a compact laser array using microresonators.

References

[1] K. D. Djordjev, S. J. Choi, S. J. Choi, and P. D. Dapkus, "Microdisk Tunable Resonant Filters and Switches", *IEEE Photon. Technol. Lett.*, vol. 14, no. 6, pp. 828-830, Jun. 2002.

[2] K. D. Djordjev S. J. Choi, S. J. Choi, and P. D. Dapkus, "Vertically coupled InP microdisk switching devices with electroabsorptive active regions", *IEEE Photon. Technol. Lett.*, vol.14, pp. 1115-1117, Aug. 2002.

[3] K. D. Djordjev, S. J. Choi, S. J. Choi, and P. D. Dapkus, "Gain trimming of the resonant characteristics in vertically coupled InP microdisk Switches", *Appl. Phys. Lett.*, vol. 80, pp. 3467-3469, May. 2002.

[4] S. J. Choi, K. D. Djordjev, S. J. Choi, and P. D. Dapkus, "CH4-based dry etching of high Q InP microdisks", *J. Vac. Sci. Technol. B*, vol. 20, pp. 301-305, Jan. 2002.

[5] S. J. Choi, Z. Peng, Q. Yang, S. J. Choi, and P. D. Dapkus, "Tunable microdisk resonators vertically coupled to bus waveguides using epitaxial regrowth and wafer bonding techniques", *Appl. Phys. Lett., submitted*, 2003.

[6] S. J. Choi, K. D. Djordjev, S. J. Choi, P. D. Dapkus, W. Lin, G. Griffel, R. Menna, and J. Connolly, "Microring resonators vertically coupled to buried heterostructure bus waveguides", *IEEE Photon. Technol. Lett., submitted*, 2003.

Eight channel microresonator MUX / DEMUX with 1.6 nm channel spacing.

In this work, we designed a multiplexer / demultiplexer that consisted of eight resonators each of which were coupled to one common waveguide and a second waveguide. The resonators were designed with a range of physical radii that shifted the absolute resonances and the free spectral ranges of the resonators so that one and only one resonance from each resonator occurred in a band 7 x 1.6 nm wide. Under these circumstances, a manifold of eight wavelengths separated by 1.6 nm that is presnt in the common waveguide will be separated spatially into the eigth output waveguides, i.e. the WDM signal will be demultiplexed. Conversely, were the resonant wavelengths inserted into the non-common waveguides of the resonators designed for each wavelength, the eight wavelengths would be combined (multiplexed) into the common waveguide. Since each of these microresonator can in principle be made tunable and switchable, this device could also be viewed as an array of modulators that individually modulates one of the eight design wavelengths from the manifold. Thus we have designed a very flexible and useful component for a WDM system. A comparable device fabricated with conventional technology, e.g. an array waveguide router, would occupy a chip area 10 X the microresonator based device we demonstrated. This work was reported in a publication (IEEE PTL **16** 2517 2004) and a talk at the 2003 LEOS Annual

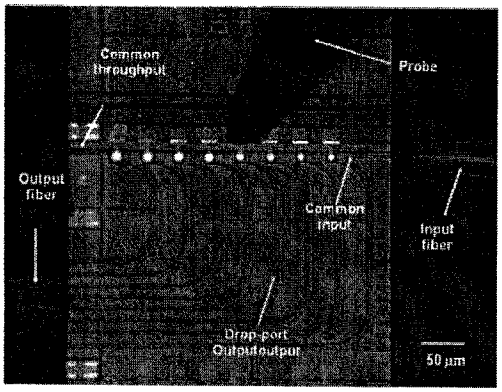

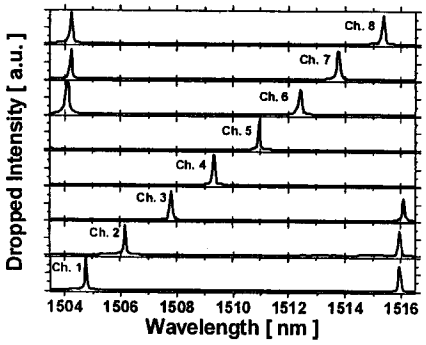

Meeting that are listed in the publications. The goals for the future are the reduction of the channel separation for such a multiplexer to 0.8 nm. This will require a multiplexer design that involves a multipole resonator element to achieve the necessary isolation between channels.

Tunable, high Q ring resonator filter with Vernier tuning over a wide range.
Many applications call for a narrow band tunable filter. The bandwidth of the resonances can be characterized by the Q of the resonator. The vertically coupled resonators that have been the subject of our work to date have Q limited by sidewall roughness and coupling of about 8000-10000. This results in a channel bandwidth of ~ 0.2 nm. These channel resonances can be tuned over 2.0 nm by the injection of free carriers into the active region. We investigated a new design for a filter element based on ring resonators that are cladded with InP to minimize the scattering. In order to minimize the radiation losses in a resonator with low lateral optical confinement, the radius of the resonator must be increased significantly to about 150-200 μm. Because we are burying the waveguide in InP, the coupling between the resonator and the waveguide can be accomplished laterally because the separation between them can be increased to one micron – a physical distance that can be defined optically using the fabrication tools at our disposal. As a result resonator coupler design was implemented using a lateral design in epitaxial materials with a transparent waveguide. Using this design we have demonstrated resonators with loss dominated Q's exceeding 10^5 and bandwidths of ~1.8 GHz. During this year we considered the very small free spectral range that results with a large radius resonator. To increase the free spectral range of the filter we designed a second order filter comprised of two rings with different radii. These rings were either directly coupled to one another by mutual coupling or coupled to one other by an intermediate waveguide (cascade coupling). In the latter case the transfer characteristic is the product of the transfer characteristics of the two resonators. More importantly, the combined filter has resonances only when two rings have a mutual resonance. This has the effect of increasing the FSR of the cascade resonator and more

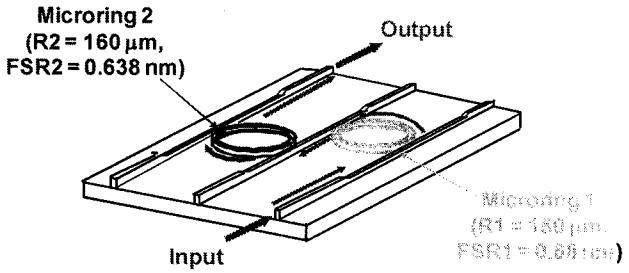

Schematic of Vernier tuned cascade filter.

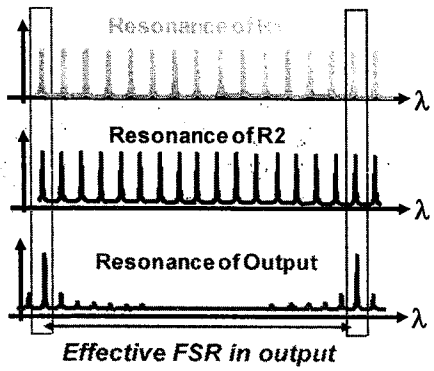

Schematic illustration of Venier expansion of FSR on cascaded resonators with different FSR's.

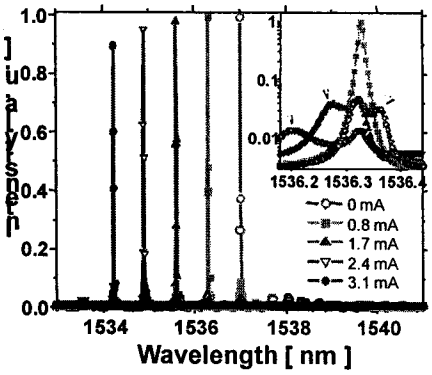

Tunable operation of cascaded pair.

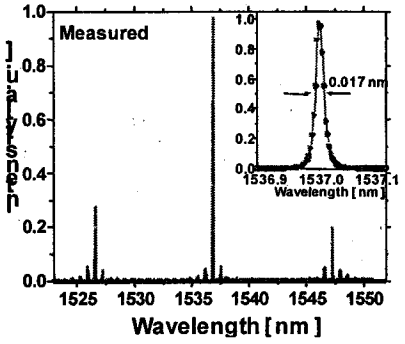

Measured Vernier expansion of FSR in cascaded pair of resonators.

importantly making the filter tunable by tuning the resonacnes of the two resonators with respect to one another. Using this design we were able to demonstrate a widely tunable (50 nm) narrow band (2GHz) filter. This Vernier filter is a general purpose element that can be used in a variety of applications such as tunable lasers and tunable receivers.

Tunable laser designs based on BH resonator filters

In the second year of the program, we demonstrated a tunable laser based on adding active gain regiosn to the input and output waveguides of a Vernier tunable filter. Though this design produced a tunable laser, it had many shortcomings, the most glaring of which was low efficiency. We have explored several new concepts for the tunable laser utilizing resonators as part of the cavity. The goal of the designs was to achieve wide tunability and to minimize losses and extraneous pumping in the cavity. The major technical challenge was the integration of the gain region in the epitaxial structure. This challenge was accomplished by two different techniques: Selective area growth and selective removal of offset quantum wells. In selective area growth the wafer surface is masked by a dielectric in certain areas. Since there can be no growth on the dielectric mask area, the local vicinity of the wafer experiences excess growth owing to the migration and diffusion of reactants from the masked area. By careful design using the models developed by Sang Jun Choi in our group, the enhance growth can be used to shift the bandgap of quantum wells to lower energy in the vicinity of the masked region. We have also used offset QW designs in which the QW are positioned at the top of the waveguide core. The first epitaxial growth is performed to complete the waveguide core. The quantum wells are removed from the regions of wafer that are to be transparent and the top cladding layer is then gorown to complete the structure. These regions are then used as the gain regions for the laser and the reminder of the waveguides on the wafer are transparent to the light generated in the enhanced growth region. We have developed mask designs for a number of different laser concepts. In some cases the active regions are actually included into the resonators themselves. In other cases the gain region in placed in straight waveguide sections. The pictures below illustrate some of the designs we explored.

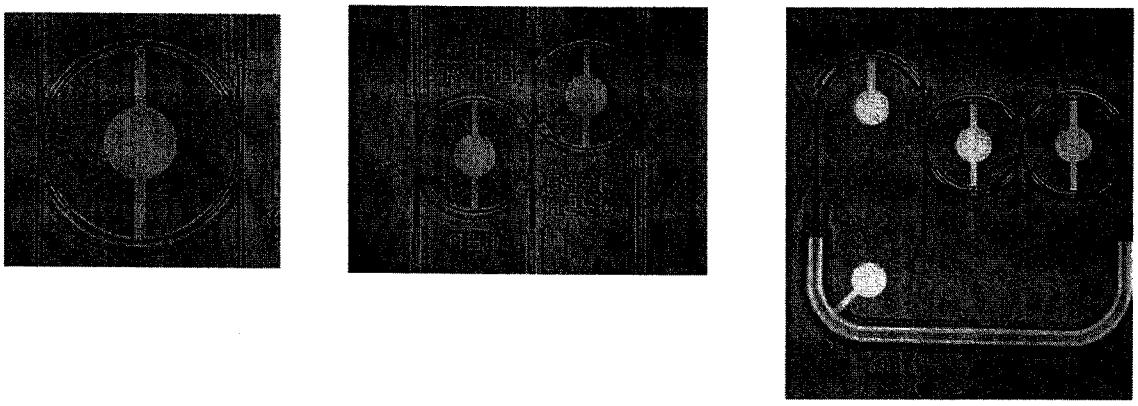

Resonator based tunable laser designs. *Left: simple resonator with gain regions; Center: Vernier filter with gain regions in waveguides; Left Vernier filter laser cavity with evanescent output coupling.*

Hi Q resonator implemented by incorporating gain in the resonator to overcome losses

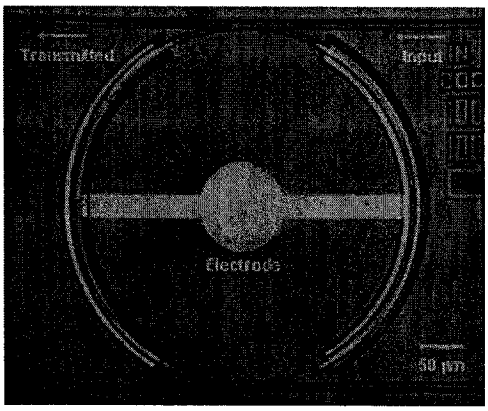

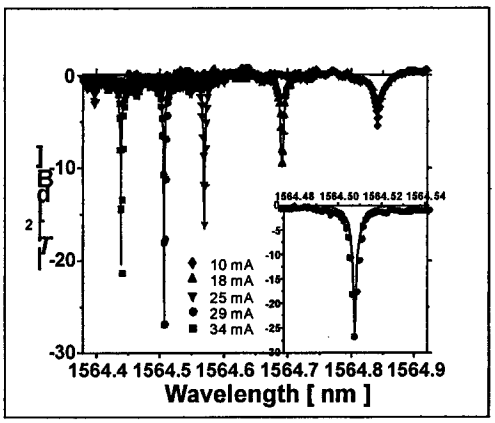

In view of the fact that our tunable laser designs have gain regions selectively incorporated into the waveguides of the devices, we investigated the possibility of creating a very high Q resonator by incorporating gain to offset absorption and scattering losses in the resonator. The resonator was designed to have a coupling limited Q of about 2x 10^4. Because the gain region is lossy when not

Ring Resonator with offset QW gain regions

Tuning characteristics of resonator with gain to compensate losses. A Q of 200000 is achieved

pumped we were unable to verify the passive characteristics of the resonator. Under forward bias we were able to achieve Q's as high as 200,000. The resonator was operated near critical coupling at an SOA current of 29 mA, which yields a coupling-limited of 2 0x10^5 with an extinction of -26 dB at the resonant wavelength. These are the highest performance resonators of their type ever demonstrated.

Semiconductor Tunable Lasers Using a Wavelength Selective Reflector Based on Ring Resonators
Resonators can be configured to act as reflectors for a laser cavity. Multiple resonators mutually coupled to one another can serve as a retroreflector at the resonances. If the coupled resonators have different free spectral ranges, they can be configured to reflect only one or a few wavelengths in the gain band. We have designed Vernier mutually coupled resonators that will reflect only a single wavelength within the gain spectrum of the laser. In addition because the resonator FSR can be tuned by current injection this reflected wavelength can be tuned to create a tunable laser. We have used our high Q resonator technology to create tunable lasers that are tunable over the entire gain spectrum of the laser.
The picture below shows the design of laser we chose to explore. The paper submitted to OFC describes

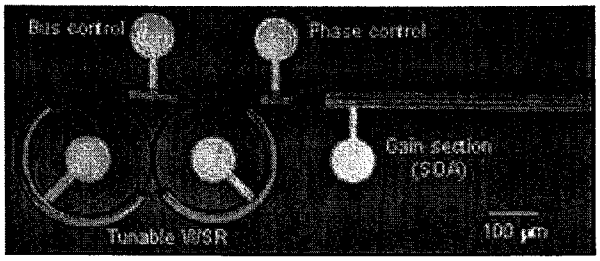

Picture of a tunable laser formed by using tunable resonator based reflectors.

the device results.

16 Channel Tunable Receiver with 100 GHz Channel Spacing and > 1Gb/s Bandwidth

Network architectures based on the gigabit Ethernet protocol often require rapid (<1 msec) reconfiguration. MIT Lincoln Laboratory is developing and planning to fly such a network as part of DARPA's Chip Scale Wavelength Division Multiplexing (CSWDM) program. To implement a fully optical implementation of a multichannel gigabit Ethernet network, LL requires a tunable receiver with rapid reconfiguration timing that is capable of serving as the receiver for a 16 channel network with 100 GHz channel spacing. This paper describes an approach to building a monolithically integrated receiver utilizing newly developed tunable filter technology at USC. The filters are based on buried ring resonator technology that has been used recently to demonstrate compound resonator tunable filters in the 1.55 micron spectral region with high throughput and potentially high channel isolation. Since the filters utilize an all-epitaxial technology, it is possible to integrate the optical amplifiers, filters and detectors seamlessly into one device in a compact footprint.

Tunable Receiver Concept

The conceptual block diagram for the proposed receiver is illustrated in Figure 1. The receiver consists of four elements; a fiber coupling mode converter, an optical amplifier, a tunable optical filter and a detector. These will all be integrated monolithically using a buried heterostructure platform onto a chip with an area < 500 x 500 microns^2. The mode converter will be designed to minimize the coupling losses

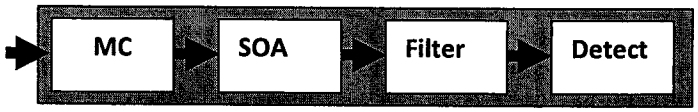

Schematic Diagram of Tunable Receiver

between the fiber and the chip and will be constructed using a vertical coupling mode converter platform developed at USC that is compatible with the rest of the elements on the chip. The optical amplifier will be designed using offset quantum wells integrated into the chip bus waveguides to achieve the necessary gain to overcome fiber coupling and on-chip losses and will serve as a gain element for higher bit rate designs in the future. The tunable filter will be fabricated from buried heterostructure ring resonator technology developed at USC and recently demonstrated with tuning over > 10 FSRs. Finally, the detector will be a waveguide coupled InGaAs PIN detector. A schematic of the chip is shown below.

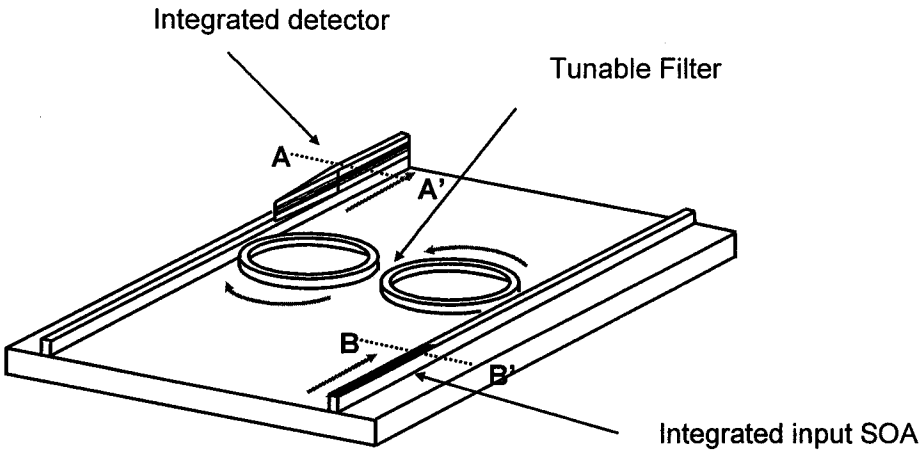

Schematic diagram of tunable receiver based on buried microring resonators.

The platform that is suggested for the proposed receiver has recently been demonstrated by USC as a platform technology for high Q resonators for signal processing and narrow line laser applications. The resonators are buried heterostructure (BH) ring resonators that have low scattering and absorption loss by virtue of the small index contrast of the resonators and the small free carrier losses. The waveguide buses and the ring resonators are constructed from a common quaternary epitaxial layer that is patterned to form the resonators and the laterally coupled bus waveguides. After patterning, the circuit is buried in InP to form the BH structure for both the resonators and the buses and to form the InP lateral coupling region. Owing to the low index contrast between the resonator and the surrounding medium, the lateral coupling distance is of order 1 μm. This can easily be patterned by conventional lithography. These resonators have demonstrated the highest Q of any known semiconductor resonators as a result. They have been employed in tunable mutually coupled and cascade resonator configurations that exhibit wide tuning with low power input by the injection of free carriers into the resonators. The two resonators are chosen to have somewhat different radii (and thus free spectral ranges) to cause a rejection of resonances not mutually present for both resonators by the Vernier effect. Figure 3 shows an example of a mutually coupled and cascade coupled Vernier BH resonators with electrical contacts applied and with integrated SOA's in the bus waveguides. These filters exhibit the classic transfer function responses on the mutual resonance as shown in Figure 4. The mutually coupled filter exhibits a lower distortion transfer function owing to the mutual coupling. Each of the resonators can be tuned by the injection of free carriers into the structure over a wide tuning range (> 5nm) as shown in Figure 5 where we show the tuning of one of the resonators across 10 free spectral ranges of the other. By tuning the second resonator

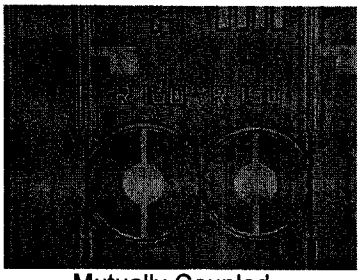
Mutually Coupled

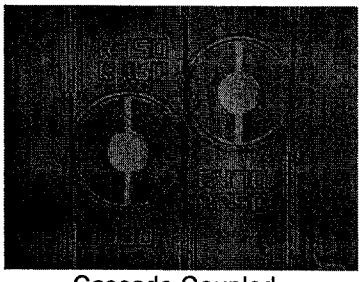
Cascade Coupled

Micrographs of mutually coupled and cascade coupled buried mirroring resonators.

simultaneously with the first we expect that tuning over a much wider range can be achieved in a manner similar to that used in sampled grating tunable lasers. The bandwidth of the filter is controlled by the coupling and losses of the microrings. Mutually coupled filters have been demonstrated with bandwidths of 5GHz. With stronger coupling the bandwidth can be increased at the expense of poorer isolation from adjacent channels.

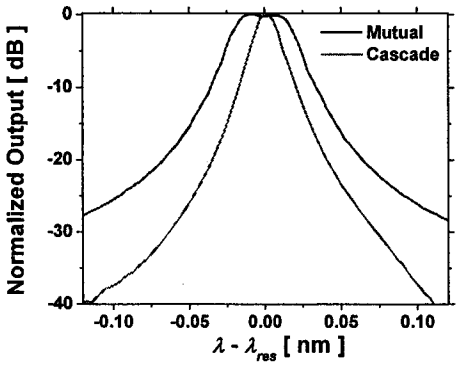

Measured transfer function responses of mutually and cascade coupled high Q BH filters.

Adjacent channel isolation can be controlled by adjusting the finesse, F (where F = FSR/ $\Delta\lambda$) of the resonators employed. The limit placed on such control is the radiation losses of the buried resonators. As the rings are made smaller to increase the FSR, the Q of the resonator decreases and the bandwidth, $\Delta\lambda$, increases. The experimental limit on the finesse for this technology has not been experimentally measured. In the absence of enough control by adjustment of F, higher order filters may be required. In the current filter designs the 100 GHz. channel isolation is calculated to be 15 dB for a 2 GHz bandwidth. We anticipate increasing the filter FSR and bandwidth while increasing the isolation.

Integrated SOA's

Semiconductor optical amplifiers can be integrated into either the bus or resonator parts of the structure by incorporating offset quantum wells (QW) at the top of the waveguide layer. These wells can be removed where not needed by selective etching prior to the InP burying process.

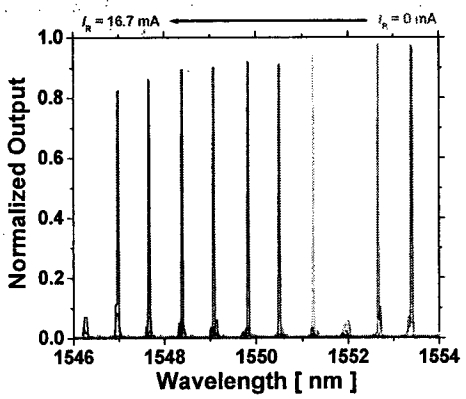

Tuning characteristics of a mutually coupled resonator Vernier filter over 10 FSR's of the laraer rina.

We anticipate incorporating a QW SOA at the input of the device to serve as a signal boost to overcome input coupling losses and possibly the resonator losses. It may also be desirable to incorporate some gain into part of the resonator to internally cancel losses caused by the injection of free carriers. This may be accomplished by leaving some of the QWs in all parts of the resonator to provide a small gain component to the tuning or all of the QWs may be incorporated in a portion of the resonator and be separately addressed and controlled. We have accomplished both of these approaches successfully.

The Detector

The waveguide detector will be incorporated into the output bus of the device. The detector will likely be incorporated by using an upper layer formed during the burying of the waveguides. Light will be coupled in to the detector by vertical coupling from the bus waveguide . Figure 6 shows the mode distribution cross section for the bus and detector regions indicted in Figure 2. The vertical coupling is achieved without reflection by tapering the detector waveguide. This design allows us to incorporate the most efficient detector into the receiver design. Integration of the detector may also be accomplished with the QWs that will be grown as the top layers of the bus waveguide. To increase the absorption of these wells the detector region is reverse biased to extend the absorption edge longer wavelength using the quantum confined Stark effect. Alternatively, by using selective area growth during the growth of the bus waveguide layers the QW width in the active region can be increased thereby shifting the absorption edge to longer wavelength. Each of these options will be assessed early in the activity to choose the one with highest performance detector that can be made with high yield.

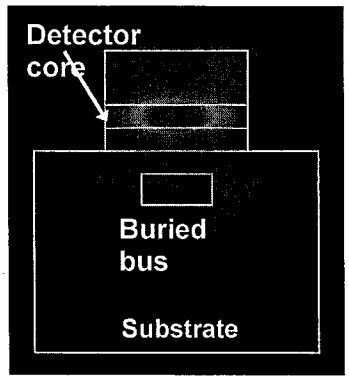

The optical mode in the detector, A-A'

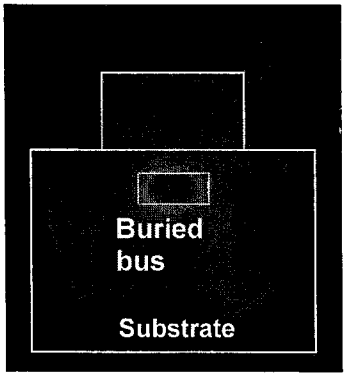

The optical mode in the bus line, B-B'

Optical Mode profiles in the sections of Fig. 2 indicated.

Technology Development Toward Multipole Filters

During this program we have consistently observed that buried heterostructure waveguides produce lower loss presumably owing to the reduced scattering on the sidewalls of the structures. We have also observed that bent rib waveguides and resonators in contact with the InP substrate exhibit excessive loss owing to light leakage from the guiding structures into unguided modes in the substrate. Both of these phenomena are ultimately detrimental to the operation of the compact filters and other devices we hope to enable with this technology. As a result we explored some approaches to reduce the leakage effects we have observed and modeled.

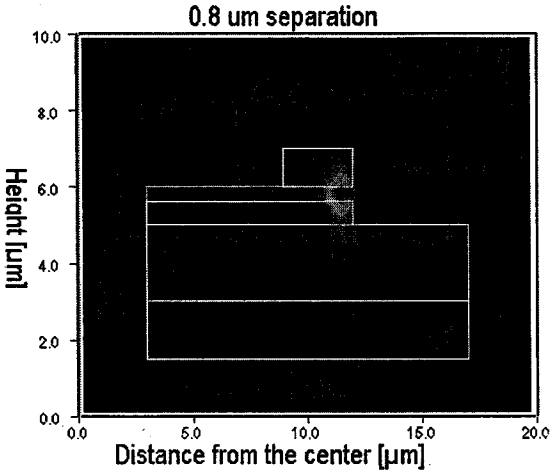

Cross sectional simulation of the mode in an air-guided resonator in contact with a high index substrate. Note the penetration of the mode into the substrate

Light leakage from bent rib waveguides and resonators in contact with the substrate arise from the reduction of the effective index of the mode in narrow waveguides and circular structures. As the rib of a waveguide is made small enough to support a single mode only, the effective index of the mode is reduced to a value comparable to that oi the InP substrate that supports the mode. As a result, light from the waveguide tends to "leak" into the substrate. The same thing occurs in an air-guided resonator in contact with a high index substrate. The first figure illustrates this leakage for a resonator. Although the mode is mostly confined to the waveguide region, a portion of the mode is seen to be penetrating the substrate and escaping as a radiation mode. This leakage limits the loss of our rib waveguides to 3 cm^{-1} and the losses in our ~10µm radius resonators to ~20 cm^{-1}. These losses can be reduced by further separating the waveguide from the substrate but the waveguides become physically unstable and the depth of etching required in the resonator causes the etching to destroy the underlying waveguide.

During this year we explored a few approaches to reduce this light leakage. Among them were to place a low index layer under the resonator or waveguide by oxidizing InAlAs and to increase the effictive index of the mode by cladding the resonator or waveguide ina lower index material. Our modeling suggested an index of 2.5 would be ideal to confine the mode and to allow us to more easily accomplish our other goal of this year – to mutually couple resonators.

We explored the use of non-stoichiometric SiN_x as a cladding for resonators and waveguides. We were able to achieve indices of refraction in the right range by adjusting the deposition conditions but we found that the indices of refraction of these materials were not stable in air. As a result we discontinued that approach. From a survey of know materials, it appears that CdS would be an ideal material to consider but we had no means to deposit this material.

We also explored the use of the oxide of InAlAs as a means to isolate the mode from the substrate. $In_{48}Al_{52}As$ is lattice matched to InP and therefore would be a good choice to incorporate into an epitaxial layer structure. However, this compound is not easily oxidized at moderate temperatures. We found that we could laterally oxidize as much as a few microns of materials within an epitaxial structure but only at temperatures ot which InP itself was unstable. Oxidizing the InAlAs caused significant degradation of the InP physical structure around the layer. The figure and table below summarize these efforts.

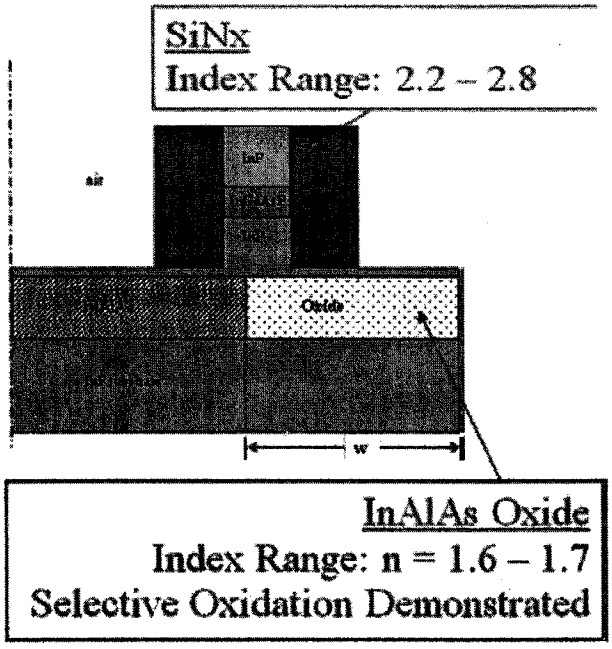

Preferred Index of refraction

Isolation Layer <2.5 CdS or InAlAs Oxide
Cladding Layer 2.5 CdS or SiN_x

InAlAs Oxide
Index Range: n = 1.6 – 1.7
Selective Oxidation Demonstrated
Buried Oxide Layers Demonstrated
InP Protection Demonstrated
Oxidation Temperature : 475C - 525C

SiN_x
Index Range: 2.2 – 2.8
Temperature Range: 200C

Our efforts to achieve a higher order filter function also involved exploration of new fabrication methods. We decided to implement these in a resonator design in which the resonator is coupled to buried heterostructure waveguides. The latter was chose to achieve lower losses in the waveguide regions. The higher order filter function is required in order to meet the requirements of the program to create filters and demultiplexers with 0.8 nm channel separation and with greater than 30 dB isolation between channels. The figures below show the effects of increasing the number of mutually coupler resonators in maximally flat design on the sharpness of the channel fall-off and the suitability of the filter to achieve the required isolation. A three pole filter is the minimum required to achieve the required isolation. The challenge in achieving this mutual coupling is the physical separation between the resonators to attain the needed coupling coefficient. The physical separation required is ~ 0.3 μm. This cannot be achieved by the lithography we have been using and requires the use of electron beam lithography. An additional challenge posed by this small separation is the need to achieve very high aspect ratio etching of the resonators. The total thickness of the resonator waveguide structure is

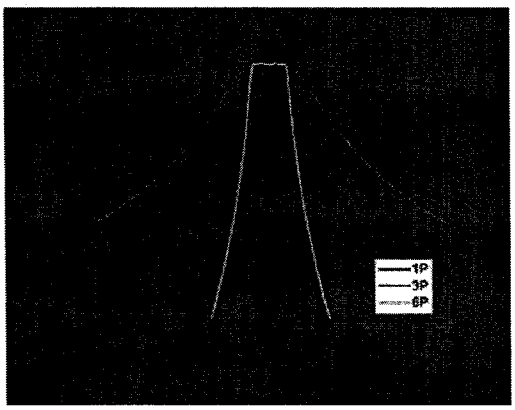

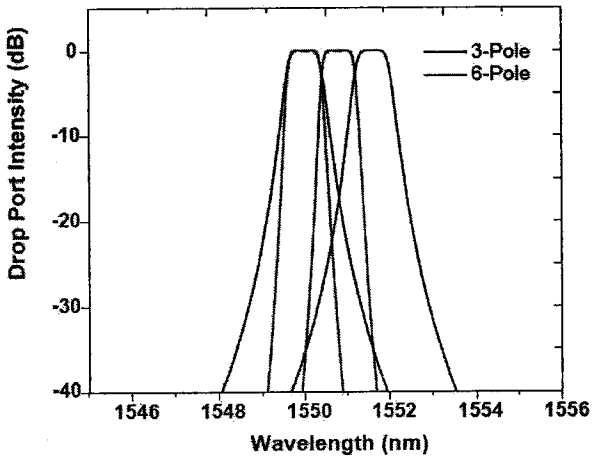

approximately 3 μm. As a result to achieve the physical separation we desire between mutually coupled resonators, we will be required to etch the resonator patterns and separations while maintaining an aspect ratio of more than 10:1. In attempting to develop these techniques we had to explore a range of new etching parameters and new resonator designs.

Two new design and fabrication issues were explored in route to developing the vertically coupled mutipole filter designs. Because the etching of the resonators is done after the epitaxial growth of the entire struct5ure, there is a need to protect the waveguides during the etching of the resonators lest the top cladding be etched from the waveguide. To accomplish this we developed a maqsk design that resulted in the waveguides being covered in the regions away from the coupliung region during the resonator etch. We then developed a selective etch to remove the cover after the resonator etching was complete. Because the design would require that large fields be defined by the lithography, we developed a process for integrating both photo and e-beam lithography. This allowed us to expose only critical regions by e-beam lithography. Integration was a challenge. The photoresist seemed to interfere with the removal of the e-beam resist and developing alignment marks for the patterns that could be detected by the e-beam system was a difficult task. Because there was no layer to layer alignment on the system at USC (a converted SEM), we were forced to develop the processes at remote laboratories (In this case, UCLA.) In spite of these difficulties, we were able to demonstrate physical models of three pole structures as are shown in the figure below.

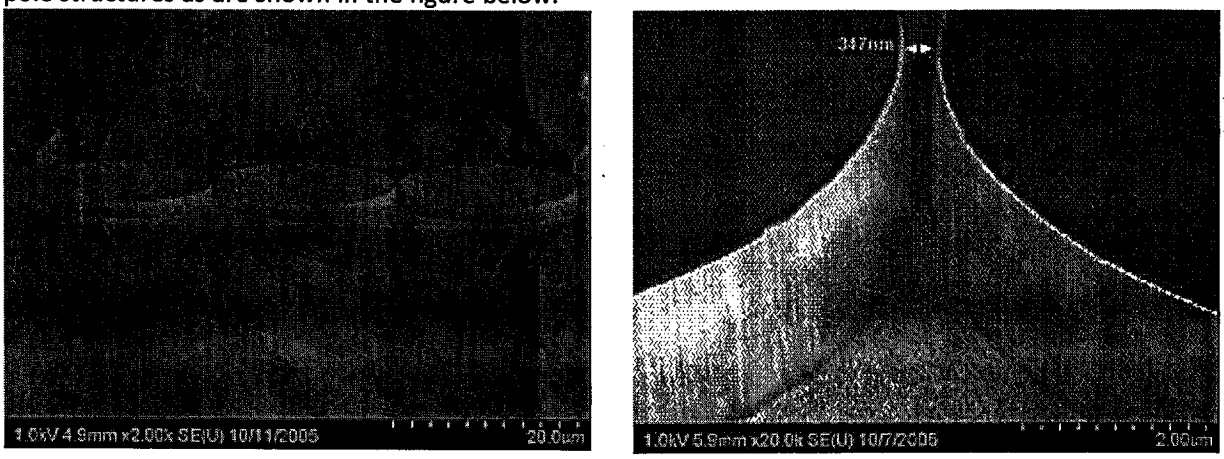

SEM micrographs of a three pole mutually coupled resonator structure (left) and an expanded view of the mutual coupling regions showing a coupling distance of 0.347 μm. (right)

Racetrack Resonators

We investigated of use racetrack resonator designs to permit longer coupling regions that might, in turn, allow us to use wider separations between the waveguides to achieve the desired coupling coefficient. Although the coupling coefficient decreases exponentially with separation, our calculations indicated that waveguide – resonator coupling could be achieved using photolithography by using ridge waveguides in the coupling region, extending the coupling distance and increasing the waveguide separation to ~1.0 μm. Such separations can be patterned using conventional photolithography. Mutual coupling of the appropriate strength can be achieved with ridge waveguides whose separations are 2.8 μm. The challenge in this approach is to transition from ridge waveguides to rib waveguides in the curved regions so that the lateral confinement can be increased enough to utilized small radius turns. Although were able to make those transitions, the abruptness of the transitions was too great and significant scattering occurred at the transitions. Fig. 5 illustrates a design based on racetracks with 75

μm long lateral coupling regions. The transfer characteristics of these devices were quite poor and inadequate for the application. Owing to our effort in this part of the project we decided to focus on disk resonators that are vertically coupled to BH waveguides for the final efforts in the program.

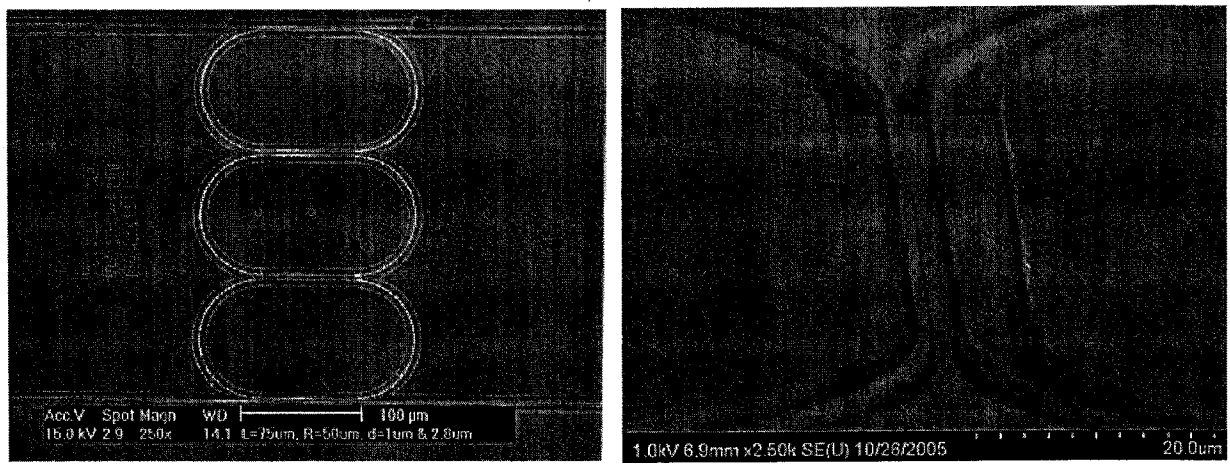

Three pole structure based on racetrack resonators. The waveguides in the coupling regions are ridge waveguides and in the curved regions are rib waveguides. $L_{couple} = 75\ \mu m$, $d_{main} = 1\ \mu m$, $d_{mutual} = 2.8\ \mu m$.

All-epitaxial Semiconductor Microresonators Vertically Coupled to Buried Bus Waveguides – A Review of our progress.

The advances in optical communication network have driven the need for all-optical dense wavelength division multiplexing (DWDM) systems. Future semiconductor device technologies are expected to realize large scale photonic integrated circuits (PICs), in which miniaturized versions of all functional components of DWDM system, such as lasers, modulators, filters, multiplexers/demultiplexers (MUX/DEMUX), and detectors, are optically inter-connected and monolithically integrated on a chip. In contrast to conventional fiber-optic WDM system manually assembled by inter-connecting individual optical modules using fiber, integrated photonic system allows reduced power consumption, compact size and improved robustness. However, technological obstacles in the integration of low loss optical waveguide inter-connections and active components have hindered the manufacturability of complex photonic integrated circuits.

A microresonators coupled to bus waveguides is a viable candidate for building-block element in PICs, due to the wide range of functionalities achievable from its wavelength selectivity and resonant enhancement. Circular microresonators, i.e., microdisks and microrings, offer compact feature size and do not require grating or facet cleaving for optical feedback, and thus are particularly suitable for monolithic integration of the aforementioned functionalities. Various material systems, such as GaAs/AlGaAs, InP/InGaAsP, polymer, and silicon-on-insulator (SOI), have been investigated to realize microresonator based devices, ranging from lasers [1-2], filters [3-6], switches [7-8], modulators [9-12], and MUX/DEMUX [13-14]. Among them the III-V semiconductor material systems with the advantage of readily available optical gain, add functionalities such as lasers and electrically tunable filters.

In actual PICs, microresonator devices make use of straight bus waveguides to couple light in and out of the resonator, and thus are primarily categorized by the coupling geometry between the resonator and the bus waveguide. Lateral and vertical couplings are the two main categories exploited. The coupling geometry is an important design parameter in choosing the right device technology. In laterally coupled microresonator structures, the resonator and the bus waveguides lie in the same epitaxial plane. The coupling is accomplished by: 1) lateral evanescent coupling between high index contrast, narrow width (<0.5μm) rib waveguides [3, 8]; 2) lateral evanescent coupling between low index contrast buried heterostructure (BH) waveguides [5]; 3) racetrack with ridge waveguides (RWG) connected to deeply etched bending curves [15]; 4) racetrack with MMI coupler [16]. The lateral coupling geometry enables monolithic integration, but also put some constraints on the fabrication process. First, using narrow rib waveguides in high index contrast, defining and etching coupling gaps on the order of 0.1 μm is highly process-dependent, making it difficult to achieve reproducible device performance; and using racetrack or BH waveguides results in large device dimensions limited by the coupler length or the bending loss of the BH waveguide. Second, the fact that the resonator and the bus waveguides are in the same epilayer places a constraint on the material design and processing flexibility which, for instance, limits the ability to integrate active functionalities.

The vertical coupling geometry enables reproducible coupling coefficient which is well controlled by epitaxially growing the coupling layer between the resonator and the bus

waveguide. In addition, the high refractive-index semiconductor coupling layer relaxes the fabrication tolerance compared to the low index coupling medium such as air in the lateral geometry. The fact that the resonator and bus waveguides reside in different epilayers makes it possible to optimize their structure, composition and corresponding dimensions independently. This is especially advantageous in the design and fabrication of active devices. It is for this reason that the vertically coupled structure has been exploited rigorously over the past decades. Three-dimensional microresonators vertically coupled to air-guided bus waveguides have been fabricated using a wafer bonding technology that requires a direct thermal fusion method [17], [2], [4] or a polymer bonding layer [18]. A wide range of InP/InGaAsP based microresonator devices have been demonstrated including laser arrays [19], modulators [10]-[11], tunable filters [7] and MUX / DEMUX [13].

Although wafer bonding is quite successful for vertically coupled microresonator structures, it hampers the large scale device manufacturability in two folds: 1) it is not monolithic, and 2) the bus waveguides are subject to large sidewall scattering loss and weak mode guiding for missing its top cladding as a result of the vertical resonator etching. Recently, an all-epitaxial technology for microresonators vertically coupled to buried heterostructure I/O bus waveguides was demonstrated [20]. The BH bus waveguides design reduces the sensitivity to the sidewall imperfections that cause scattering losses, and provides good electrical and thermal paths to the substrate in active devices [21]. A carefully engineered two-step planarization regrowth process was developed to form a flat resonator structure on top of the buried bus waveguides, enabling a potentially robust technology platform for monolithic PICs. However, the air-guided microresonator directly attached to a high index substrate suffered large power leakage to the substrate. In addition, the phase mismatch between the resonator and the buried bus waveguides makes the vertical coupling inefficient. This work addresses these problems, and demonstrates low loss air-guided microdisks vertically coupled to low loss buried bus waveguides employing a unique fabrication process featuring selective area deep etching with multi-level mask. Since optical gain can be easily incorporated into the waveguides, this all-epitaxial technology facilitates complex integration of various DWDM functionalities using microresonator based devices inter-connected by low loss bus lines.

This paper is organized as follows. Section 0 summarizes the results from our previous work, based on which we have optimized the microresonator waveguide structure in order to reduce the substrate leakage loss and enhance the vertical couplings, as shown in Section 0. In Section 0, we demonstrate the development of a unique fabrication process featuring selective area deep etching with multi-level mask, which enables further suppressing of the leakage from the resonator to the substrate while preserving low loss buried bus waveguides. Finally we present the improved device performance in Section 0.

PRELIMINARY RESULTS

In the vertical coupling configuration, the microresonators must lie on top and in close proximity to the buried bus waveguides, Fig. 1. The planarity of the microresonator layer is crucial for minimizing scattering loss. Even minor variations in the planarity of the resonator layer can result in scattering that is detrimental to the device performance. In practice, however, it is extremely difficult to planarize layers regrown on mesas or rib-type waveguides with conventional metal-organic chemical vapor deposition (MOCVD) within the very thin layer thickness required for optical coupling. Therefore, a carefully engineered two-step regrowth

process was developed in [20]. In this approach, first, the empty space between the etched rib bus waveguides was filled by InP utilizing selective area regrowth (SAG) with an optimized V/III ratio; next, the SiN_x mask on the bus waveguide was removed, and a second regrowth was followed to build vertically stacked microresonator waveguide layers on top of the buried bus waveguides.

A small radius (R = 10μm) microring resonator vertically coupled buried heterostructure (BH) bus waveguides was fabricated to verify the planarity of the regrowth. The typical quality factor (Q) was measured to be ~2500. The estimated microring loss, $\alpha \sim 20cm^{-1}$, was mainly attributed to the mode leakage through the high-index substrate. More analysis suggested that better phase or index matched microresonator and bus waveguide can produce the same desired coupling coefficient with a larger vertical separation, which helps reduce the substrate leakage loss.

Another demonstration was carried out using the combination of planarization regrowth and wafer bonding techniques [21]. In this experiment, low loss ($\sim 0.5cm^{-1}$) from the mostly buried bus waveguide and an improved thermal and electrical conduction from the microresonator to the substrate were confirmed. The latter benefit resulted in a 40% enhancement in the resonance tuning efficiency and a wider tuning range by free carrier injections, compared to the microdisk devices made by the wafer-bonding technology. However, the microdisk loss was > $20cm^{-1}$ for similar reasons, i.e., resonator mode leakage to the substrate.

DEVICE DESIGN

The cross-section of a microdisk vertically coupled to buried bus waveguides is shown in Fig. 2. The single mode bus waveguides are 0.4μm thick by 0.8μm wide undoped InGaAsP (Q1.1μm) and buried in n-doped InP, The undoped InGaAsP disk waveguide is separated from the buried buses by an n-doped InP coupling layer with thickness of d_{cpl}, and on top is a 1μm thick p-type InP disk cladding layer that has a graded doping concentration in order to reduce free carrier absorption in the microdisk. The microdisk radius varies from 8μm to 12μm.

PHASE MATCHING BETWEEN WAVEGUIDE MODES

The challenges for microresonators vertically coupled to buried bus waveguides were identified from the preliminary results: (1) large leakage loss from the microresonator to the high-index substrate, and (2) inefficient vertical coupling between the microresonator and the bus waveguide. Both problems can be attributed to the large phase mismatch between the two waveguides.

In our previous demonstration in **Error! Reference source not found.**, the disk core was 0.4μm thick layer of InGaAsP having bandgap of Q_{disk} = 1.25μm. The effective disk modal index was n_{disk_eff} = 3.074, while that of the buried bus waveguide was n_{bus_eff} = 3.170, close to the index of bulk InP. Clearly, n_{disk_eff} should be increased to match n_{bus_eff}. Here, both a higher index material and a thicker layer are considered for the disk waveguide core. A 0.6μm thick Q1.35μm InGaAsP layer is chosen. Further increase in the waveguide thickness results in multi-mode operation near the wavelength of interest (1550nm), and further increase in the material index leads to excessive material absorption loss. Consequently, n_{disk_eff} is increased to 3.145, which is <1% mismatched to n_{bus_eff}. Table 1 summarizes the modifications in the effective modal indices.

LOSS IN MICRODISKS

A full vectorial mode solver, OlympIOs, was used to calculate the microdisk modal fields. The disk waveguide structures before and after optimization were compared. The separation d_{sep} between the disk core and the substrate was varied in each case. The software accounts for bending losses, α_{bend}, and leakage loss to substrate, α_{sub}, but not scattering loss, α_{scat}. Since α_{bend} is negligible in this strongly confined structure (lateral index step $\Delta n = n_{disk} - n_{air}$), the calculated results show mostly the effect of α_{sub} The disk loss can be reduced by an order of magnitude using the optimized disk waveguide structure, as can be seen from Fig. 3. The reduction in substrate leakage is visually noticeable in Fig. 4, for d_{sep} = 0.8μm. Another observation from Fig. 3 is that α_{sub} is exponentially dependent on d_{sep}. It becomes negligible when the disk mode is sufficiently separated from the substrate, which suggests α_{sub} can be further reduced by deeper etching of the microdisk.

COUPLING BETWEEN WAVEGUIDES

The vertical resonator-to-bus coupling was calculated using the coupled mode theory for curved waveguides implemented by a 5th-order Runge-Kutta method **Error! Reference source not found.**. The optimized disk structure showed coupling about two times higher than our previous result from the structure in [21], as shown in Fig. 5. Moreover, in the preliminary demonstration, the coupling layer thickness d_{cpl} was larger than optimal as a compromise in order to suppress the disk mode leakage to the substrate. In Section 0, a novel fabrication process is developed to preserve the coupling region while deeply etching the microdisk in other parts using a multi-mask, self aligned etching process, so that d_{cpl} and d_{sep} are not correlated. In this experiment, the coupling layer thickness d_{cpl} is chosen to be 0.63μm to achieve input coupling $\kappa_{in} \sim 8.6\%$.

LOSS IN BUS WAVEGUIDES

Owing to its small cross-section, the single mode bus waveguide is very sensitive to sidewall imperfections. This sensitivity is greatly relieved in a buried structure because the scattering loss is strongly dependent on the index contrast [23]. Secondly, for active or tunable devices, the overall *p-i-n* diode structure for electrical conduction is formed through the *n*-InP surrounding the buried bus (Fig. 2), rather than directly through the *n*-doped bus as in the wafer bonding devices **Error! Reference source not found.**. This way the bus waveguide can be undoped, avoiding the additional carrier absorption loss.

One major concern in this technology is that the top cladding of the bus waveguide will be sacrificed during the standard microdisk vertical etching, which results in a vertically asymmetric buried bus waveguide mode whose intensity profile is pushed toward the substrate. This problem is also resolved using the novel etching process that is discussed in the next section.

DEVICE FABRICATION

To initiate the process, a 0.4μm thick InGaAsP (Q1.1μm) bus waveguide layer was grown on an (001)-oriented InP substrate. A 0.2μm thick SiN_x layer was deposited on the surface as a masking layer. Stripe I/O bus patterns were defined along the [110] direction using contact photo-lithography, and 1μm wide vertical mesas were etched using BCl_3 chemistry in an inductively coupled plasma (ICP) etching process. After the bus waveguide formation, the bus mesas were buried and the wafer surface was planarized using the planarization regrowth

technique described in **Error! Reference source not found.**. After planarization, a 0.6μm thick InGaAsP (Q1.35μm) disk core layer and a 1μm thick InP top cladding layer were grown. The major challenge in the overall process is to deeply etch the microdisk while preserving the coupling layer on top of the bus waveguide to keep it well buried

1. Conventional bi-level etching:

A bi-level etching technique was presented in [15] to realize a racetrack ring laser composed of shallow RWG coupler and deeply etched bending sections. In this approach, the bus and racetrack waveguiding geometry was first etched using a metal mask, and then the coupling region was coated with a second dielectric layer and the rest of the racetrack structure was deeply etched. In our work of process development, this approach was initially attempted, but instead of using metal and dielectric as the mask combination, SiO_2 and SiN_x were used as the microdisk mask and the cover for the bus waveguide, respectively, because a smooth disk pattern was not achievable using metal mask patterned by lift-off process. To pattern the 2nd SiN_x bus cover over the 1st SiO_2 disk mask, a highly selective SiN_x-over-SiO_2 etching condition was necessary. An RIE etching condition was developed using $O_2/N_2/CF_4$ chemistry with flow rates 18/30/18sccm at pressure = 400mT and RF power = 500W. More than 40:1 SiN_x/SiO_2 selectivity was achieved, with a smooth and vertical SiN_x profile.

The bi-level etching process was carried out. First, control the etching of the microdisk so as to stop right below the disk core layer so that the whole coupling layer is untouched. Then, with the SiO_2 disk mask untouched, a SiN_x layer was deposited to cover the buried bus with a wider new mask before performing a second etch. In this way, the disk can be deeply etched using the 1st SiO_2 mask, and the buried bus is protected by the 2nd SiN_x cover. However, a physical step was present around the microdisk waveguide core due to the interrupted 2-step etching, as shown in Fig. 6. Two problems were identified: 1) the deposition of the 2nd dielectric layer enlarged the disk size since the deposition by PECVD also covered the etched disk sidewall, and 2) the top of the disk sidewall was slightly attacked during the 2nd etching.

2. Selective area deep etching with multi-level mask

To avoid the formation of the step on the disk edge, the deep disk etching should be done in a continuous fashion after all of the dielectric masks are formed. A one-step etch process featuring selective area deep etching with a multi-mask was developed, as illustrated in Fig. 7.

A 2-mask combination was patterned by first forming a SiO_2 bus cover mask and then a SiN_x disk mask. The previously developed $O_2/N_2/CF_4$ selective etching recipe was applied in pattering the 2nd SiN_x mask. Note that the SiN_x disk mask was formed last in order to protect it. The previously demonstrated SiN_x/SiO_2 selective etching was applied to achieve a smooth disk mask on top of the bus cover mask, as shown in Fig. 8.

Following the multi-mask patterning, the sample was deeply etched. It is preferable that the deep etching is not interrupted. This requires that the bus cover mask is removed at some point during this continuous etch to allow disk etching in the coupling region, as illustrated by the last step in Fig. 7. Inductively coupled plasma (ICP) using BCl_3 chemistry was applied for this step, which etches InP ~ 10 times faster than SiN_x/SiO_2. The SiO_2 cover is removed over the entire surface during the etch but the SiN_x mask preserves the disk geometry. Therefore, by carefully controlling the initial thicknesses of the dielectric masks, the majority of the microdisk was deeply etched except in the coupling region, where the etching stopped right below the

disk core layer.

The fabricated device is shown in Fig. 9, where the microdisk was etched to ~ 3.7μm deep in total, and the bus waveguides were well buried with the coupling layer InP remaining as the bus top cladding. The disk core was ~ 2μm above the etched wafer floor, allowing for virtually no mode leakage to the substrate.

RESULTS AND DISCUSSION

The transmission characteristics of the microdisks were measured by coupling an external tunable laser light into the buried bus waveguide at one facet and collecting the output signal at the other bus facet. For a 12μm radius microdisk coupled to a single buried bus waveguide, the normalized (to peak intensity) transmission spectra with a TE-polarized (out-of-wafer-plane) tunable laser input signal is given in Fig. 10. The quality factor (Q), extinction ratio (T_{min}/T_{max}), and free spectral range (FSR) are ~9000, 0.36, and ~8.85nm, respectively, from which the filter finesse (F) is estimated to be ~ 52.

Data fitting was followed to extract the effective index of the microdisk (n_{disk_eff}), the intensity loss coefficient (α), and the coupling coefficient between the disk and the bus waveguide (κ). The intensity transmission ($|t|^2$) for a single bus coupled microdisk is given by

$$|t|^2 = \left| \frac{\sqrt{1-\kappa} - e^{-\alpha l/2} \cdot e^{-j\beta l}}{1 - \sqrt{1-\kappa} e^{-\alpha l/2} \cdot e^{-j\beta l}} \right|^2 \qquad (1)$$

where $\beta = 2\pi n_{disk\_eff}(\lambda)/\lambda$ is the wave propagation constant, and $l = 2\pi R$.

The effective index n_{disk_eff} (λ=1550nm) = 3.1527 with -0.33/μm dispersion is chosen to match the FSR. Optical loss α = 2.9cm^{-1} and coupling κ = 0.085 are determined through the quality factor and the extinction ratio. The validity of κ is confirmed by its consistency to the calculation (Fig. 5), from which κ = 0.086 when the coupling layer thickness d_{cpl} = 0.63μm.

The estimated resonator loss, α = 2.9cm^{-1}, is much lower than the preliminary results (α ~ 20cm^{-1}), which indicates that the substrate leakage is effectively suppressed. The remaining loss is believed to result mainly from disk sidewall scattering. Another merit of the material system used here is that optical gain can be readily integrated to compensate for this loss.

As a result of the greatly reduced substrate leakage loss, the quality factor Q is improved from ~ 2500 to ~ 9000. Calculation shows this Q is limited by the stronger coupling. A slightly weaker κ that is matched to the disk round-trip loss can both improve the extinction ratio and reduce the resonance line-width. Nevertheless, a finesse F > 50 is a clear advance in the device's filtering capability. It is also believed that by integrating active regions in the device, the microresonators have the potential to achieve good lasing performance, considering the improved thermal and electrical conduction that was shown in the preliminary demonstration on this technology platform **Error! Reference source not found.**.

CONCLUSION

A low loss small radius all-epitaxial InP-based microdisk vertically coupled to low loss BH bus waveguides was demonstrated. Great reduction of optical loss in the microdisk and reasonable bus-to-disk coupling were achieved. Considering other benefits such as low bus waveguide loss and better thermal and electrical conduction demonstrated in our preliminary results, this technology platform is potentially important in PICs, because it combines low loss waveguides with the ability to integrate the active functionalities of III-V semiconductors.

ACKNOWLEDGEMENT

The authors would like to acknowledge Dr. Kostadin D. Djordjev for his suggestions and discussions.

REFERENCES

[1] M. Fujita, R. Ushigome, and T. Baba, "Continuous wave lasing in GaInAsP microdisk injection laser with threshold current of 40μA", *Electronics Letters*, vol. 36, no. 9, pp. 790-791, April 2000.

[2] S. J. Choi, K. D. Djordjev, S. J. Choi, and P. D. Dapkus, "Microdisk lasers vertically coupled to output waveguides", *IEEE Photon. Technol. Lett.*, vol. 10, no. 15, pp. 1330-1332, Oct. 2003.

[3] P. P. Absil, J. V. Hryniewicz, B. E. Little, R. A. Wilson, L. G. Joneckis, P.-T. Ho, "Compact microring notch filters", *IEEE Photon. Technol. Lett.*, vol. 12, no. 4, pp. 398-400, Apr. 2000.

[4] K. D. Djordjev, S. J. Choi, S. J. Choi, and P. D. Dapkus, "High-Q vertically coupled InP microdisk resonators", *IEEE Photon. Technol. Lett.*, vol. 14, no. 3, pp. 331-333, Mar. 2002.

[5] S. J. Choi, Z. Peng, Q. Yang, S. J. Choi, and P. D. Dapkus, "Tunable narrow linewidth all-buried heterostructure ring resonator filters using Vernier effects", *IEEE Photon. Technol. Lett.*, vol. 17, no. 1, pp. 106-108, Jan. 2005.

[6] B. E. Little, J. S. Foresi, G. Steinmeyer, E. R. Thoen, S. T. Chu, H. A. Haus, E. P. Ippen, L. C. Kimerling, and W. Greene, "Ultra-compact Si-SiO2 microring resonator optical channel dropping filters", *IEEE Photon. Technol. Lett.*, vol. 10, no. 4, pp. 549-551, Apr. 1998.

[7] K. D. Djordjev, S. J. Choi, S. J. Choi, and P. D. Dapkus, "Microdisk tunable resonant filters and switches", *IEEE Photon. Technol. Lett.*, vol. 14, no. 6, pp. 828-830, June 2002.

[8] V. R. Almeida, C. A. Barrios, R. R. Panepucci, and M. Lipson, "All-optical control of light on a silicon chip", *Nature*, pp. 1081-1084, Oct. 2004.

[9] P. Rabiei, W. H. Steier, C. Zhang, and L. R. Dalton, "Polymer Micro-ring Filters and Modulators", *IEEE J. Lightwave Technology*, vol. 20, no. 11, pp. 1968-1975, Nov. 2002

[10] T. Sadagopan, S. J. Choi, S. J. Choi, and P. D. Dapkus, "Carrier-induced refractive index changes in InP-based circular microresonators for low-voltage high-speed modulation", *IEEE Photon. Technol. Lett.*, vol. 17, no. 2, pp. 414-416, Feb. 2005.

[11] A. Stapleton, S. Farrell, Z. Peng, S. J. Choi, L. Christen, J. O'Brien, P. D. Dapkus, and A. Willner, "Low V_π modulators containing InGaAsP/InP microdisk phase modulators", *Appl. Phys. Lett.*, 90, 161121, 2007.

[12] Q. Xu, S. Manipatruni, B. Schmidt, J. Shakya, and M. Lipson, "12.5 Gbit/s carrier-injection-based silicon micro-ring silicon modulators", *Optics Express*, vol. 15, no. 2, pp. 430-436, 22 January 2007.

[13] S. J. Choi, Z. Peng, Q. Yang, S. J. Choi, and P. D. Dapkus, "An eight-channel demultiplexing switch array using vertically coupled active semiconductor microdisk resonators", *IEEE Photon. Technol. Lett.*, vol. 16, no. 11, pp. 2517-2519, Nov. 2004.

[14] B. E. Little, S. T. Chu, W. Pan, and Y. Kokubun, "Microring resonator arrays for VLSI photonics", *IEEE Photon. Technol. Lett.*, vol. 12, no. 3, pp. 323-325, Mar. 2000.

[15] G. Griffel, J. H. Abeles, R. J. Menna, A. M. Braun, J. C. Connolly, and M. King, "Low-threshold InGaAsP ring lasers fabricated using bi-level dry etching", *IEEE Photon. Technol. Lett.*, vol. 12, no. 2, pp. 146-148, Feb. 2000.

[16] D. G. Rabus, and M. Hamacher, "MMI-coupled ring resonators in GaInAsP-InP", *IEEE Photon. Technol. Lett.*, vol. 13, no. 8, pp. 812-814, Aug. 2001.

[17] D. V. Tishinin, I. Kim, C. Lin, A. E. Bond, and P. D. Dapkus, "Novel fabrication process for vertical resonant coupler with precise coupling efficiency", *Proc. IEEE 11th Annual LEOS Meeting*, San Francisco (CA), TuK5, pp. 93-94, Oct. 1998.

[18] R. Grover, P. P. Absil, V. Van, J. V. Hryniewicz, B. E. Little, O. King, L. C. Calhoun, F. G. Johnson, and P.-T. Ho, "Vertically coupled GaInAsP-InP microring resonators", *Opt. Lett.*, vol. 26, no. 8, pp. 506-508, Apr. 2001.

[19] S. J. Choi, Z. Peng, Q. Yang, S. J. Choi, and P. D. Dapkus, "Eight-channel microdisk CW laser arrays vertically coupled to common output bus waveguides", *IEEE Photon. Technol. Lett.*, vol. 16, no. 2, pp. 356-358, Feb. 2004.

[20] S. J. Choi, K. D. Djordjev, S. J. Choi, P. D. Dapkus, W. Lin, G. Griffel, R. Menna, and J. Connolly, "Microring resonators vertically coupled to buried heterostructure bus waveguides", *IEEE Photon. Technol. Lett.*, vol. 16, no. 3, pp. 828-830, Mar. 2004.

[21] S. J. Choi, Z. Peng, Q. Yang, S. J. Choi, and P. D. Dapkus, "Tunable microdisk resonators vertically coupled to bus waveguides using epitaxial regrowth and wafer bonding techniques", *Appl. Phys. Lett.*, vol. 84, no. 5, pp. 651-653, Feb. 2004.

[22] K. D. Djordjev, Ph. D. dissertation, University of Southern California, USA, 2002.

[23] J. P. R. Lacey and F. P. Payne, "Radiation loss from planar waveguides with random wall imperfections", *IEE Proc. Pt. J.*, vol. 137, no. 4, pp. 282-288, August 1990.

FIGURE CAPTIONS

Fig. 1 Schematics of a microdisk vertically coupled to buried bus waveguides.

Fig. 2 Cross-section of a microdisk vertically coupled to buried bus waveguides. d_{sep} is the separation between the disk and the substrate; d_{cpl} is the coupling layer thickness between the disk and the bus waveguide.

Fig. 3 Calculated loss of an air-guided microdisk (R = 10μm) vertically separated from the substrate by d_{sep}. The optimized disk structure (filled square) shows loss ~10 times lower than the preliminary structure (open circle).

Fig. 4 Calculated modal field distribution in a 10μm radius microdisk using (a) 0.4μm thick Q1.25μm InGaAsP, and (b) 0.6μm thick Q1.35μm InGaAsP on an InP substrate. d_{sep} = 0.8μm. The substrate leakage is clearly suppressed in the optimized waveguide.

Fig. 5 Calculated vertical coupling coefficient between an air-guided microdisk (R = 10μm) and a buried bus waveguide separated by a d_{cpl} thick InP coupling layer. The optimized disk structure (filled square) shows two times higher coupling than the preliminary structure (open circle).

Fig. 6 SEM image of a microdisk formed by a standard 2-step etching. The physical step was a result of two separate etchings.

Fig. 7 Process flow of selective area deep etching of a microdisk vertically coupled to buried bus waveguides with layered SiN_x/SiO_2 masks.

Fig. 8 SEM image of a SiN_x disk mask on top of a SiO_2 bus cover mask showing the 2-mask process. A smooth SiN_x disk mask was achieved.

Fig. 9 SEM image of a deeply etched microdisk vertically coupled to buried bus waveguides with thick top claddings.

Fig. 10 Measured (dotted line) and calculated (solid line) transmission spectra of a 12μm radius microdisk vertically coupled to a single buried bus waveguide. TE-polarized tunable laser is coupled to the input bus waveguide. R = 12μm, n_{disk_eff} = 3.1527 at λ = 1550nm, dispersion = -0.33/μm, κ = 0.085, and α = 2.9cm^{-1} are used in the calculation to fit the measured data.

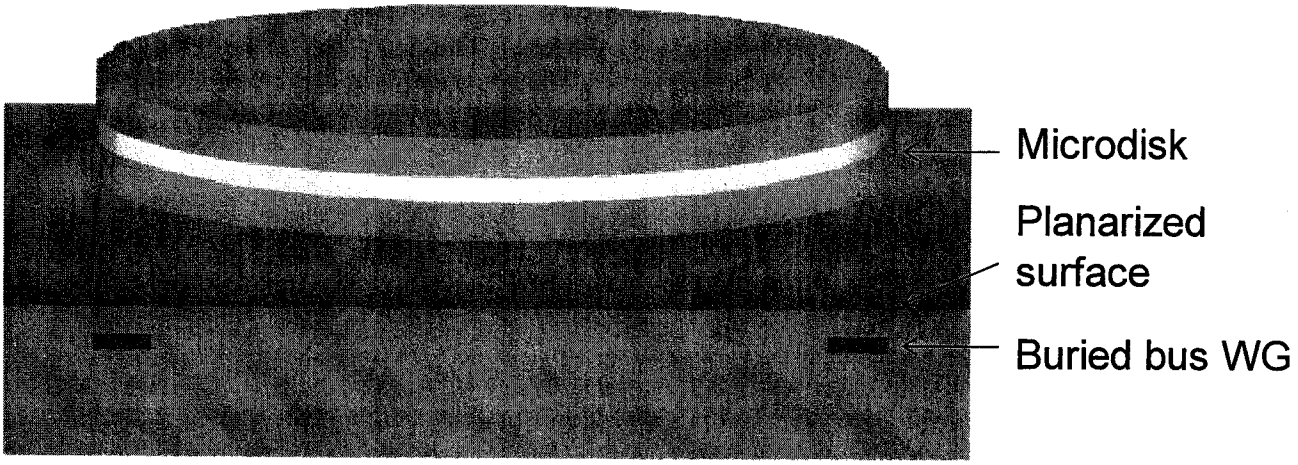

Fig. 1

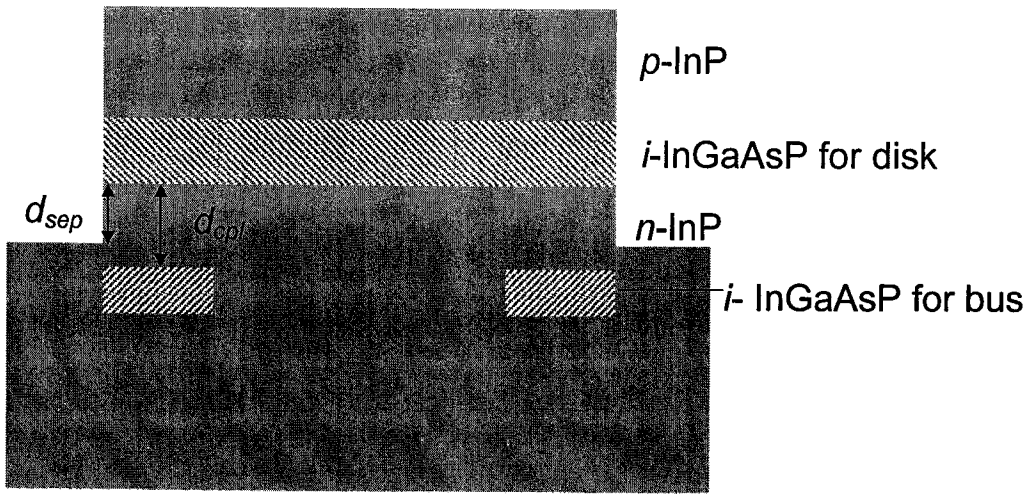

Fig. 2

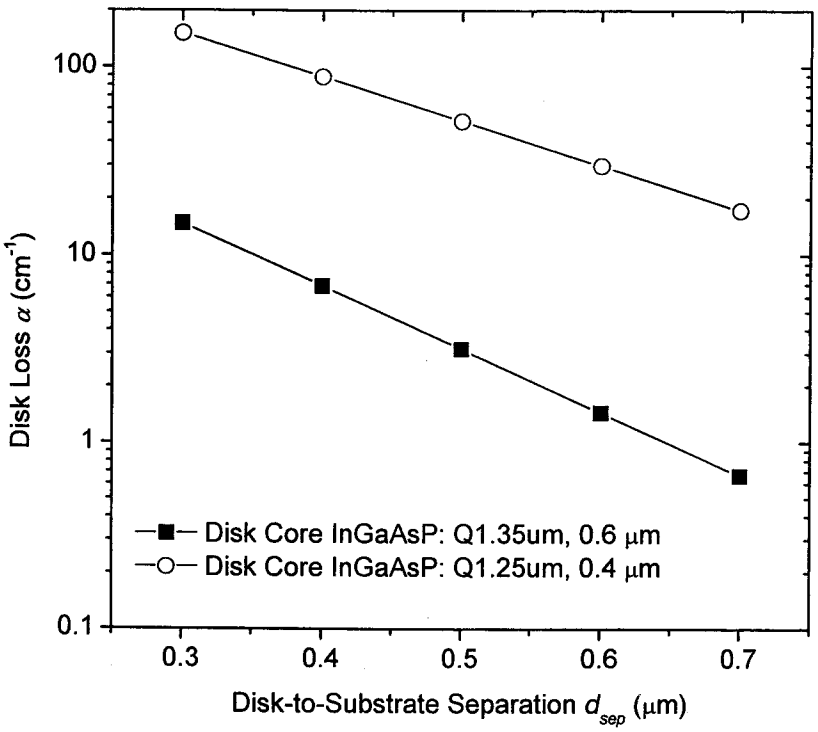
100
10
1
0.1
Disk Loss α (cm-1)
0.3
0.4
0.5
0.6
0.7
Disk-to-Substrate Separation dsep (μm)
Disk Core InGaAsP: Q1.35um, 0.6 μm
Disk Core InGaAsP: Q1.25um, 0.4 μm

Fig. 3

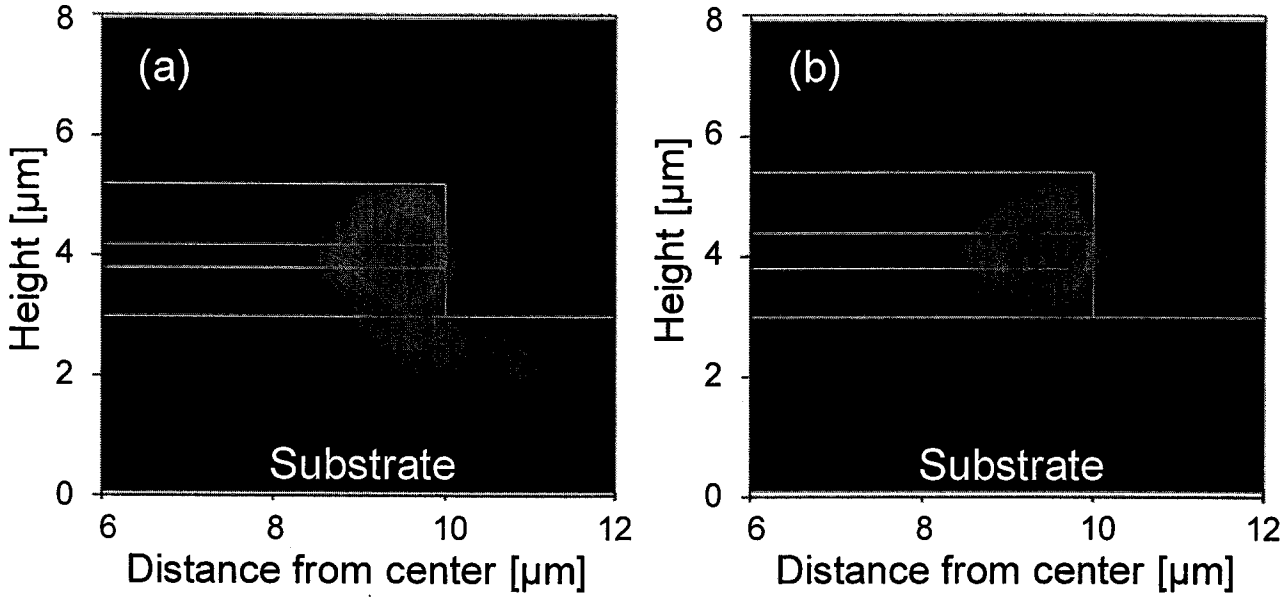

Fig. 4

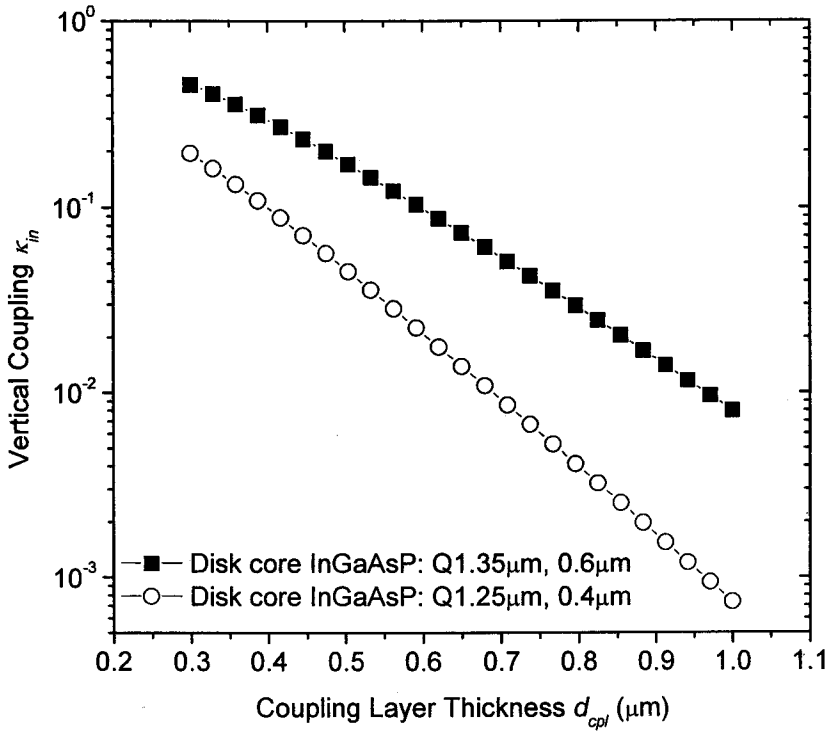
Vertical Coupling κ_{in}
10^0
10^{-1}
10^{-2}
10^{-3}
Disk core InGaAsP: Q1.35μm, 0.6μm
Disk core InGaAsP: Q1.25μm, 0.4μm
0.2
0.3
0.4
0.5
0.6
0.7
0.8
0.9
1.0
1.1
Coupling Layer Thickness d_{cpl} (μm)

Fig. 5

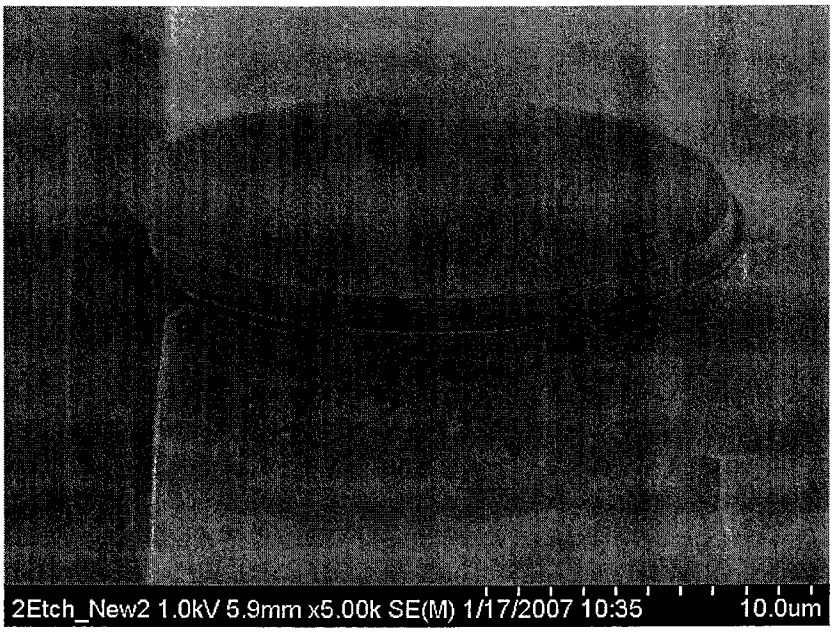

Fig. 6

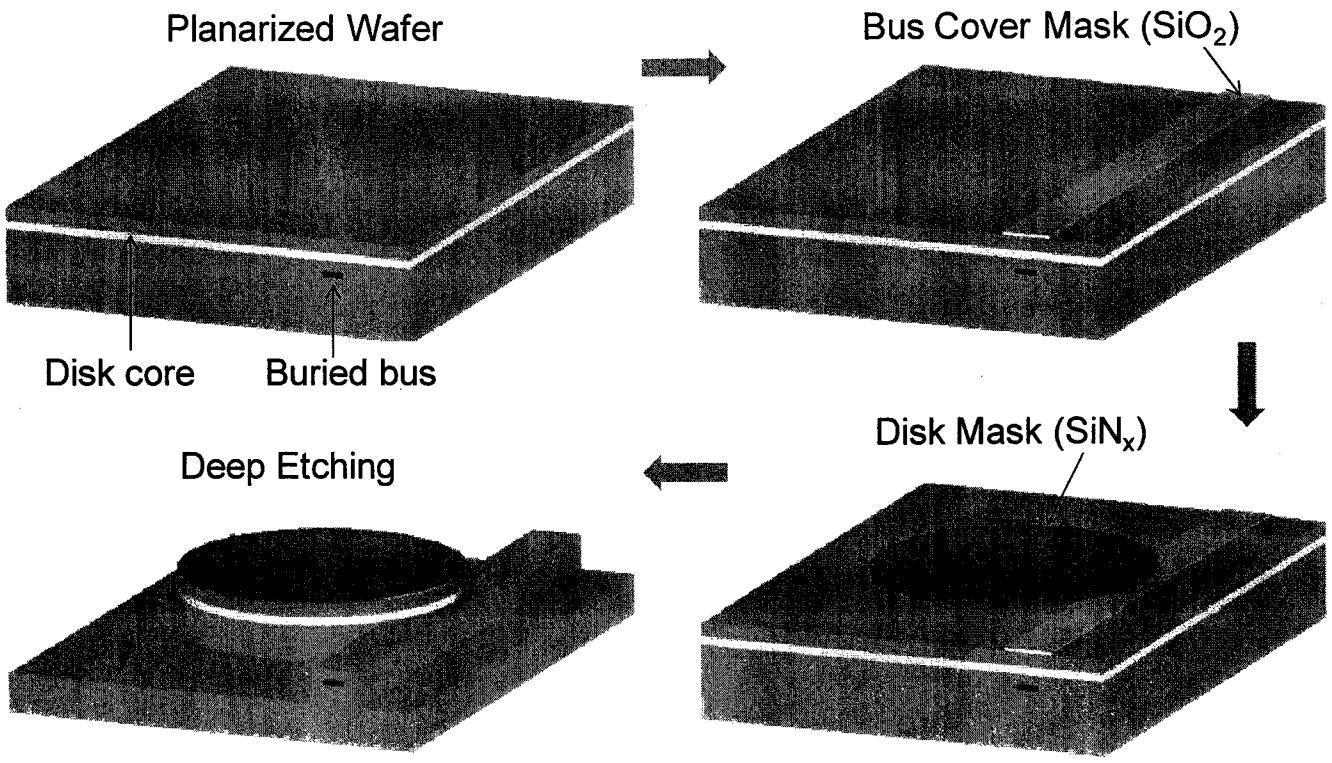
Planarized Wafer
Bus Cover Mask (SiO_2)
Disk core
Buried bus
Disk Mask (SiN_x)
Deep Etching

Fig. 7

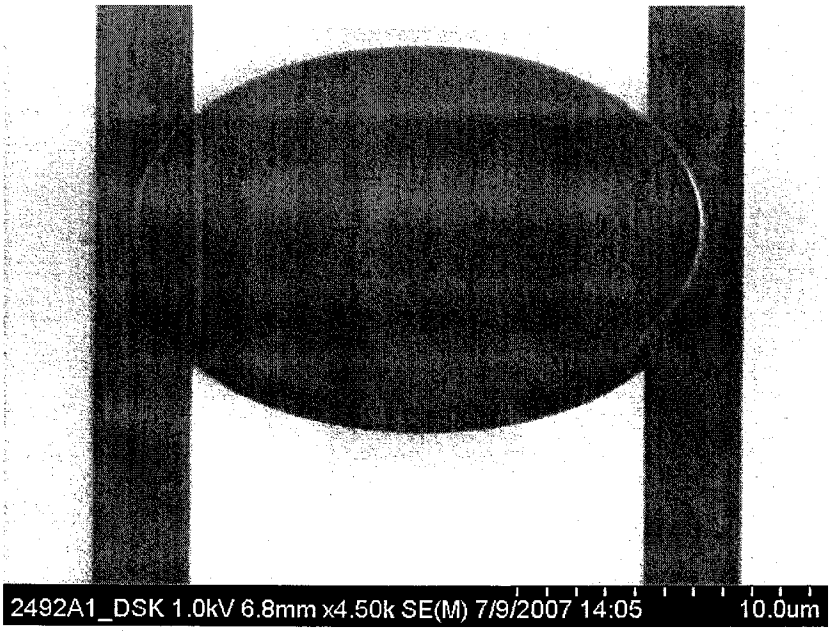

Fig. 8

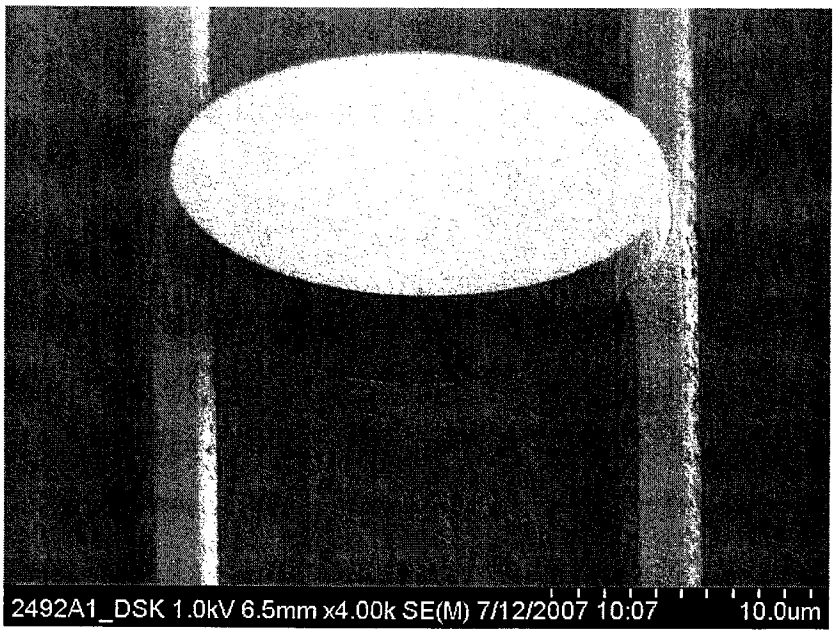

Fig. 9

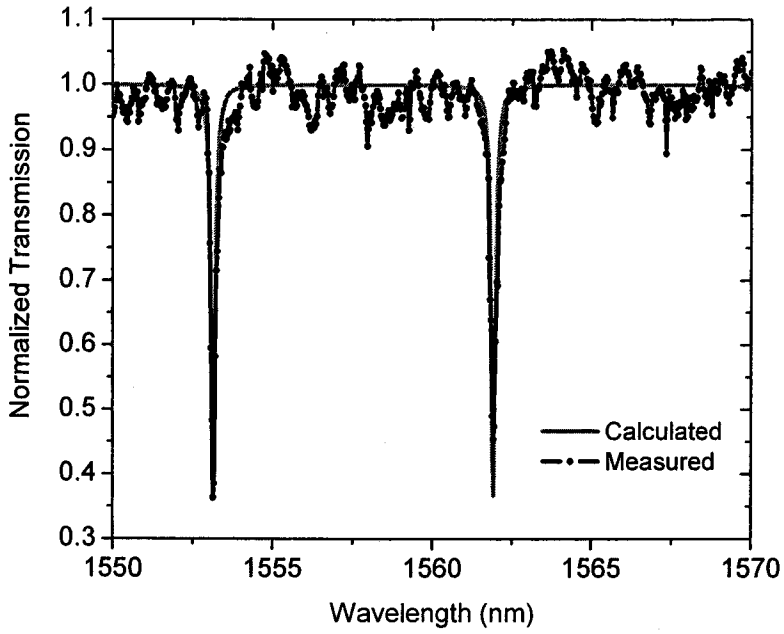
Normalized Transmission
1.1
1.0
0.9
0.8
0.7
0.6
0.5
0.4
0.3
1550
1555
1560
1565
1570
Wavelength (nm)
Calculated
Measured

Fig. 10

Table 1 Calculated waveguide effective modal indices. The optimized microdisk structure is almost phase matched to the buried bus waveguide.

	Waveguide Structure	Effective Modal Index
Buried bus WG	0.4μm thick, 0.8μm wide InGaAsP (Q1.1μm) buried in InP	n_{bus_eff} = 3.170
Air-guided microdisk (*R* = 10μm)	0.4μm thick InGaAsP (Q1.25μm)	n_{disk_eff} = 3.074
	0.6μm thick InGaAsP (Q1.35μm)	n_{disk_eff} = 3.145

Microresonator and Photonic Crystal Filters, Lasers, and Modulators for Analog and Digital Chip Scale WDM Systems

Final Report

John O'Brien
P. Daniel Dapkus

Table of Contents

Refereed Journal Papers

1. M. H. Shih, Mahmood Bagheri, Adam Mock, S. J. Choi, J. D. O'Brien, P. D. Dapkus, Wan Kuang,"Identification of modes and single mode operation of sapphire-bonded photonic crystal lasers under continuous-wave room temperature operation," *Applied Physics Letters* **90** 121116 (2007).

2. Tian Yang, Adam Mock, John D. O'Brien, Samuel Lipson, Dennis G. Deppe, "Lasing characteristics of InAs quantum dot microcavity lasers as a function of temperature and wavelength," *Optics Express* **15**(12) 7281-7289 (2007).

3. Tian Yang, Adam Mock, John D. O'Brien, Samuel Lipson, Dennis G. Deppe, "Edge-emitting photonic crystal double-heterostructure nanocavity lasers with InAs quantum dot active material," *Optics Letters* **32**(9) 1153-1155 (2007).

4. M. H. Shih, Adam Mock, M. Bagheri, N.-K. Suh, S. Farrell, S.-J. Choi, J. D. O'Brien, P. D. Dapkus,"Photonic crystal lasers in InGaAsP on a SiO2/Si substrate and its thermal impedance," *Optics Express* **15**(1) 227-232 (2007).

5. M.H. Shih, A. Mock, M. Bagheri, N.-K. Suh, S. Farrell, S.-J. Choi, J. D. O'Brien, P. D. Dapkus, "Photonic crystal lasers in InGaAsP on a SiO_2/Si substrate and its thermal impedance", *Optics Express*, **15**, pp. 227-232 (2006).

6. M.-H. Shih, W. Kuang, A. Mock, M. Bagheri, E.H. Wang, J. D. O'Brien, P. D. Dapkus, "High Quality Factor Photonic Crystal Heterostructure Laser," *Appl. Phys. Lett.*, **89**, 163115 (2006).

7. W. Kuang, W.J. Kim, A. Mock, J. D. O'Brien, "Propagation Loss of Line-Defect Photonic Crystal Slab Waveguides", *IEEE J. Sel. Top. Quant. Elect.*, **12**, pp. 1183-1195 (2006).

8. M. Bagheri, M.-H. Shih, W. K. Marshall, Z.-J. Wei, S. J. Choi, J. D. O'Brien, P. D. Dapkus, "Linewidth and modulation response of two-dimensional microcavity photonic crystal lattice defect lasers," *IEEE Phot. Tech. Lett.*, **18,** pp. 1161-1163 (2006).

9. M.-H. Shih, Wan Kuang, Tian Yang, Mahmood Bagheri, Zhi-Jian Wei, S.-J. Choi, Ling Lu, John D. O'Brien, P. Daniel Dapkus, "Experimental Characterization of the Optical Loss of Sapphire-Bonded Photonic Crystal Laser Cavities", *IEEE Phot. Tech. Lett.***18**, pp. 535-537 (2006).

10. T. Yang, J. D. O'Brien, S. Lipson, D. G. Deppe, "InAs Quantum Dot Photonic Crystal Lasers and Their Temperature Dependence," *IEEE Phot. Tech. Lett.*, **17**, pp. 2244-2246 (2005).

11. W. Kuang, J. R. Cao, S.-J. Choi, J. D. O'Brien, P. D. Dapkus, "Modified Suspended Membrane Photonic Crystal D3 Laser Cavity with Improved Side Mode Suppression Ratio," *IEEE Phot. Tech. Lett.*, **17,** *pp. 941-942,(2005)*

12. M. H. Shih, W. J. Kim, Wan Kuang, J. R. Cao, S. J. Choi, J. D. O'Brien and P. D Dapkus, "Experimental Characterization of the Reflectance of 60-degree Waveguide Bends in Photonic Crystal Waveguides," *Appl. Phys. Lett.*, 86, pp. 191104-1–191104-3 (2005)

13. Wan Kuang, Jiang R. Cao, Tian Yang, Sang-Jun Choi, Po-Tsung Lee, John D. O'Brien, P. Daniel Dapkus "Classification of Modes in Suspended Membrane 19-Missing Hole Photonic Crystal Microcavities,," *J. Opt. Soc. Am. B.*, 22, pp. 1092-1099, (2005).

14. J.-R. Cao, Wan Kuang, Zhi-Jian Wei, Sang-June Choi, Haixia Yu, M. Bagheri, J. D. O'Brien, P. D. Dapkus, "Sapphire-Bonded Photonic Crystal Microcavity Lasers and Their Far-Field Radiation Patterns," *IEEE Phot. Tech. Lett.*, **17**, 4 (2005).

15. Wan Kuang, John D. O'Brien, "Reducing the out-of-plane radiation loss of photonic crystal waveguides on high-index substrates," *Optics Letters*, **29**, (8) pp. 860, Apr 15 (2004).

16. Woo Jun Kim ; O'Brien, J.D., "Optimization of a two-dimensional photonic-crystal waveguide branch by simulated annealing and the finite-element method," *Journal of the Optical Society of America B (Optical Physics)*, **21** (2), 289-95 (2004).

17. M. H. Shih, W. J. Kim, Wan Kuang, J. R. Cao, H. Yukawa, S. J. Choi, J. D. O'Brien, P. D. Dapkus, W. K. Marshall, "Two-dimensional photonic crystal Mach-Zehnder interferometers," Appl. Phys. Lett., **84**, pp. 460-462 (2004).

18. J. R. Cao, Wan Kuang, Sang-Jun Choi, Po-Tsung Lee, John D. O'Brien, and P. Daniel Dapkus, "Threshold dependence on the spectral alignment between the quantum-well gain peak and the cavity resonance in InGaAsP photonic crystal lasers," *Applied Physics Letters* **83**, 4107-4109(2003).

19. Woo Jun Kim, Wan Kuang, John D. O'Brien, "Dispersion Characteristics of Photonic Crystal Coupled Resonator Optical Waveguides," *Optics Express*, **11**, pp. 3431-3437 (2003).

20. W. Kuang, C. Kim, A. Stapleton, W.-J. Kim, J. D. O'Brien , "Calculated Out-of-Plane Transmission Loss for Photonic Crystal Slab Waveguides," *Optics Letters*, **28**, pp. 1781-1783 (2003).

21. W. Kuang, C. Kim, A. Stapleton, J. D. O'Brien, "Grating Assisted Coupling of Optical Fibers and Photonic Crystal Waveguide," *Optics Letters*, **27**, pp. 1604-1606 (2002).

22. J-R. Cao, P.-T. Lee, S.-J. Choi, J. D. O'Brien, P. D. Dapkus, "Lithographic Fine Tuning of VCSEL Pumped 2-D Photonic Crystal Lasers," *Journal of Nanoscience and Nanotechnology*, **2**, pp. 313-315, (2002).

23. P.-T. Lee, J.-R. Cao, S.-J. Choi, Z.-J. Wei, J. D. O'Brien, P. D. Dapkus, "Operation of Photonic Crystal Membrane Lasers Above Room Temperature," *Appl. Phys. Lett.*, **81**, 3311-3313, (2002).

Invited Presentations

1. John O'Brien, Photonic Crystal Devices," 9th International Conference on Transparent Optical Networks, July 2, 2007 Rome, Italy (LEOS Distinguished Lecture)

2. John O'Brien, "Photonic Crystal Devices," PHASE 2007 International Workshop on Physics and Applications of Semiconductor Lasers, March 28, 2007 Metz, France (keynote speaker)

3. J. O'Brien, "Photonic Crystal Lasers", 10th International Symposium on Contemporary Photonics Technology, paper A-2 Tokyo, Japan January 2007.

4. John O'Brien, M.-H. Shih, T. Yang, M. Bagheri, A. Mock, W. K. Marshall, P. D. Dapkus, D. Deppe, "Photonic Crystal Devices", paper S2.1, IEEE Nano, Cincinnati OH (July 2006) (invited).

5. Min-Hsiung Shih, Wan Kuang, Mahmood Bagheri, Adam Mock, San-Jun Choi, John D. O'Brien, P. Dan Dapkus, "High Side-Mode-Suppression-Ratio Sapphire-Bonded Photonic Crystal Laser under Continuous-Wave Operation", Integrated Photonics Research and Applications Topical Meeting, Uncasville, Connecticut, USA, 2006 (invited).

6. John O'Brien, Wan Kuang, W. J. Kim, M.-H. Shih, A. Stapleton, N.-K. Suh, S.-J. Choi, P. D. Dapkus, "Photonic Crystal-Based Waveguide Structures and Interfaces", paper FTuW1 , Frontiers in Optics 2005 Optical Society of America annual meeting , Tuscon, AZ (invited).

7. John O'Brien, "Photonic Crystal Devices", Opto Ireland 2005, Dublin, Ireland paper 5825-21, April 2005 (invited).

8. John O'Brien, "Photonic Crystal Devices," COMMAD 04, Brisbane Australia Dec. 2004 (invited).

9. John O'Brien, "Nanophotonic Devices," International Workshop on Laser Cleaning 4, Sydney, Australia, Dec, 15, 2004 (invited).

10. John O'Brien, "Photonic Crystal Waveguides for On-Chip Interconnects," OIDA Optical Interconnects - Thinking Inside of the Box, Burlingame, CA (October 22 (2004)) (invited).

11. John O'Brien, "Photonic Crystal Devices- Towards Devices on High-Index Substrates," The 4th US-Japan Joint Symposium on Nanophotonics: Beyond the Limit of Optical Technology, Tokyo, Japan (October 27, 2004) (invited).

12. John O'Brien, J.-R. Cao, W. Kuang , M.-H. Shih, W. J. Kim, A. Stapleton, Z.-J. Wei, S.-J. Choi, P. D. Dapkus, "Photonic Crystal Devices," paper FMK5,, Frontiers in Optics/Laser Science XX Conference (the 88th annual meeting of the Optical Society of America), Rochester, New York (October 2004) (invited).

13. J. O'Brien, J.-R. Cao, A. Stapleton, M.-H. Shih, Wan Kuang, W. J. Kim, Z.-J. Wei, S. –J.Choi, P. D. Dapkus, "Characterization of Photonic Crystal Structures," session III, Symposium on Optical Fiber Measurements (SOFM 2004), Boulder, Colorado (September 2004) (invited).

14. J.D. O'Brien, "Design, Fabrication, and Characterization of Photonic Crystal Waveguides," paper 5359-30, Photonics West 2004, San Jose, CA (invited).

15. J. D. O'Brien, J. Cao, W. Kuang, M. H. Shih, W. J. Kim, H. Yukawa, C. Kim, S. Choi, P. D. Dapkus, "Photonic crystal waveguides and emitters," paper 5277-32, SPIE's International Symposium on Microelectronics, MEMs, and Nanotechnology 2003, Perth Australia (invited).

16. John O'Brien, "Photonic Crystal Devices," paper WL1, LEOS Annual Meeting 2003, Tuscon, AZ (invited).

17. P. D. Dapkus, J. D. O'Brien, "Meso- and Nanophotonic Devices for Integrated Photonic Circuits," paper IV.5, Device Research Conference 2003, Salt Lake City, UT (invited).

18. John O'Brien, Jiang-Rong Cao, Wan Kuang, Min-Hsiung Shih, Woo Jun Kim, Cheolwoo Kim, Po-Tsung Lee, Sang-Jun Choi, P. D. Dapkus, "Photonic Crystal Devices," paper JWC3, Optics in Computing 2003, Washington, D.C (invited).

Refereed Conference Proceedings

1. Ling Lu, Tian Yang, Adam Mock, M. H. Shih, E. H. Hwang, Mahmood Bagheri, Andrew Stapleton, Stephen Farrell, J. D. O'Brien, P. D. Dapkus, "60 microWatts of fiber-coupled peak output power from an edge-emitting photonic crystal heterostructure laser," Conference on Lasers and Electro- Optics, May 2007, Baltimore, Maryland, USA, Paper CMV3.

2. Andrew Stapleton, Nankyung Suh Cockerham, Mahmood Bagheri, Stephen Farrell, and John O'Brien,"Silicon Photonic Crystal Directional Couplers for Power Splitting, wavelength Filtering, and Optical Switching," Optical Fiber Communication Conference (OFC), Anaheim, California, OMI4(2007)

3. A. Mock, W. Kuang, M.-H. Shih, E. H. Hwang, W. J. Kim, J. D. O'Brien, P.D. Dapkus, "Spectral Properties of Photonic Crystal Double-Heterostructure Resonant Cavities", paper ML4, LEOS, Montreal, Canada (2006).

4. M. H. Shih, M. Bagheri, A. Mock, N.-K. Suh, S. Farrell, S.-J. Choi, J. D. O'Brien, P. D. Dapkus, "Photonic Photonic Crystal Lasers in InGaAsP on a SiO2/Si Substrate", The 11th OptoElectronics and Communications Conference (OECC 2006), July 2006, Kaohsiung, Taiwan.

5. M. H. Shih, Adam Mock, E. H. Hwang, Wan Kuang, John D. O'Brien, P. Dan Dapkus, "Photonic Crystal Heterostructure Laser with Lattice-Shifted Cavity", paper CMKK3, CLEO 2006, Long Beach, CA.

6. Tian Yang, Samuel Lipson, J. D. O'Brien, D. G. Deppe, "Photonic Crystal Double-Heterostructure Nanocavity InAs Quantum Dot Laser with Waveguide Output Coupling," Conf on Lasers and Electro-Optics, CThK2, Long Beach, California, USA, 2006.

7. Tian Yang, Samuel Lipson, Adam Mock, J. D. O'Brien, D. G. Deppe, "Lasing Behavior of InAs Quantum Dot Micro-Cavities as a Function of Wavelength and Temperature," Integrated Photonics Research and Applications Topical Meeting, Uncasville, Connecticut, USA, ITuE4, 2006.

8. M.-H. Shih, W. Kuang, M. Bagheri, A. Mock, E.H. .Hwang, P. D. Dapkus, J. D. O'Brien, "Photonic Crystal Heterostructure Laser Cavity," paper TuJ7, IEEE LEOS Annual Meeting 2005, Sydney, Australia.

9. M. Bagheri, M.H. Shih, W.K. Marshall, Z.-J. Wei, S.-J. Choi, J. D. O'Brien, P. D. Dapkus, "Small-Signal Characterization of Photonic Crystal Lasers," PECS-VI International Symposium on Photonic and Electromagnetic Crystal Structures, A-7, Aghia Pelaghia, Crete, Greece, June 2005.

10. Wan Kuang, Adam Mock, John D. O'Brien, "Predicted Low-Loss Photonic Crystal Waveguides in SOI," PECS-VI International Symposium on Photonic and Electromagnetic Crystal Structures, B-57, Aghia Pelaghia, Crete, Greece, June 2005.

11. M. Bagheri, M.H.Shih, W. K. Marshall, R.J. Cao, Z.-J. Wei, S.-J. Choi, J. D. O'Brien, P. D. Dapkus , "Intensity modulation response of 2-d photonic crystal lasers bonded to sapphire" 12th European Conference On Integrated Optics, Grenoble, France,April (2005).

12. M.H. Shih, W. Kuang, Tian Yang, Mahmood Bagheri, Z.-J. Wei, S.-J. Choi, John D. O'Brien, and P. Daniel Dapkus, "Optical loss determination of sapphire-bonded photonic crystal laser cavities by varying the number of photonic crystal cladding periods," Integrated Photonics Research, paper ITuG3, San Diego, CA, (April 12, 2005).

13. Tian Yang, J. D. O'Brien, ,Samuel Lipson, D.G. Deppe, "Photonic Crystal Lasers with Quantum Dots Active Regions and Their Temperature Dependence," CLEO 2005, paper CThO4, Baltimore, Md (May 2005).

14. M.H. Shih, W.J. Kim, W. Kuang, J.-R. Cao, S.J. Choi, J. D. O'Brien and P. D. Dapkus, "Experimental Characterization of the Reflectance of 60-Degree Bends in Photonic Crystal Waveguides," paper WV5, LEOS Annual Meeting, San Juan Puerto Rico, (Nov. 2004).

15. M. Bagheri, J. R. Cao, W. K. Marshall, Z.-J. Wei, S.-J. Choi, J. D. O'Brien, P. D. Dapkus, A. Willner, "Linewidth Measurement of Sapphire-Bonded 2-D Photonic Crystal Lasers," paper MC4, LEOS Annual Meeting, San Juan Puerto Rico, (Nov. 2004).

16. Zhi-Jian Wei, J. R. Cao, Yuanming Deng, Sang-Jun Choi, Wan Kuang, John D. O'Brien, P. Daniel Dapkus, "Room temperature 1.55 μm photonic crystal lasers integrated with AlGaAs oxide aperture," FMK4, Frontiers in Optics/Laser Science XX Conference (the 88th annual meeting), Rochester, New York (October 2004).

17. J. R. Cao, Wan Kuang, Sang-Jun Choi, John D. O'Brien, P. Daniel Dapkus, "Modified Photonic Crystal D3 Laser Cavity for Improving Side Mode Suppression Ratio," paper FB2,19th IEEE International Semiconductor Laser Conference (ISLC'04), Matsue, Japan (September 2004).

18. J. R. Cao, Zhijian Wei, Sangjun Choi, Wan Kuang, John D. O'Brien, P. Daniel Dapkus, "Sapphire-Bonded Photonic Crystal Lasers," TuA-3-2, 6th International Conference on Indium Phosphide and Related Materials (IPRM'04), Kagoshima, Japan (2004).

19. Wan Kuang, J. D. O'Brien, "Photonic Crystal Devices," The International Symposium on Optical Science and Technology: SPIE 49th Annual Meeting, paper 5554-28, Denver, Co. Aug. 3 (2004).

20. J.-R. Cao, W. Kuang, Z-J. Wei, S.-J. Choi, J. D. O'Brien, P. D. Dapkus, "Far-fields of photonic crystal microcavity lasers," paper CtuR7, CLEO 2004, San Francisco, CA (2004).

21. W. Kuang, J. D. O'Brien, "Strategy for Reducing the Out-of-Plane Radiation Loss in Photonic Crystal Waveguides in High-Index Substrates," paper CWG4, CLEO 2004, San Francisco, CA (2004).

22. W. Kuang, J.-R. Cao, T. Yang, S.-J. Choi, J. D. O'Brien, P. D. Dapkus, "Classification of Modes in Multi-Moded Photonic Crystal Microcavities," paper CtuDD3, CLEO 2004, San Francisco, CA (2004).

23. M-H. Shih, W. Kuang, J.-R. Cao, S.-J. Choi, W. K. Marshall, P. D. Dapkus, J. D. O'Brien, "Two-Dimensional Photonic Crystal Mach-Zehnder Interferometers," postdeadline paper CThPDB7, CLEO 2003, Baltimore, MD.

24. T. Yang, O. Shchekin, D. G. Deppe, J. D. O'Brien "Microdisks with quantum dot active regions lasing near 1300 nm at room temperature," paper CWK3, CLEO 2003, Baltimore, MD.

25. J.-R. Cao, Z.-J. Wei, S.-J. Choi, W. Kuang, H. Yu, J. D. O'Brien, P. D. Dapkus, "Sapphire bonded photonic crystal microcavity lasers," paper TuE5, OSA Annual Meeting, Tuscon AZ (2003).

26. J. -R. Cao, P. Lee, S. Choi, J. O'Brien, P. Dapkus, "Threshold Pump Power Dependence on the Spectral Alignment Between the Gain Peak and the Cavity Resonance in InGaAsP Photonic Crystal Lasers," paper MF57, OFC 2003.

27. P.-T. Lee, J. R. Cao, S.-J. Choi, T. Yang, J. D. O'Brien, P. D. Dapkus, "Investigation of the Optical Losses in Photonic Crystal Laser Cavities by Varying the Number of Lattice Periods," paper ThB5, 2002 International Semiconductor Laser Conference, Garmisch-Partenkirchen, Germany.

28. W. Kuang, C. Kim, A. Stapleton, J. D. O'Brien, "Grating assisted coupling of optical fibers and photonic crystal waveguides," paper CMC3, CLEO 2002, Long Beach, CA.

29. J. R. Cao, P.-T. Lee, S.-J. Choi, J. D. O'Brien, P. D. Dapkus, "Lithographic Tuning of 2-D Photonic Crystal Lasers," paper TuW4, OFC 2002, Anaheim, CA.

30. C. Kim, J. O'Brien, "Maximization of transmission at branches in photonic crystal waveguides," paper ThK6, OFC 2002, Anaheim, CA.

Lasers

Mode structure in micocavities

a. Double heterostructure cavities

A significant amount of effort in the latter stages of the program went into modeling and demonstrating edge-emitting photonic crystal heterostructure laser cavities. This effort was a result of a plan, on our part, to use these lasers to demonstrate significant gains in photonic crystal output power. Our recent results include a demonstration of more than 200 μW peak output power from a micrcavity photonic crystal lasers. This amount of output power is critical if these lasers are to function as signal source in high bandwidth optical systems. A detailed three-dimensional finite-difference time-domain analysis of photonic crystal double heterostructure bound state resonances was done and compared to experimental results. The figure at left shows the calculated H_z component for the first three bound states. The connection between different photonic crystal waveguide bands and the associated photonic crystal double heterostructure bound states was made, and mode profiles were presented. We analyzed the quality factors using the Padé interpolation method and directional radiation properties by calculating the time-averaged Poynting vector. We also considered field profiles of higher order bound states and discuss cavity geometries to enhance a given bound state mode relative to neighboring modes. Experimental lasing results were obtained demonstrating the utility of our approach.

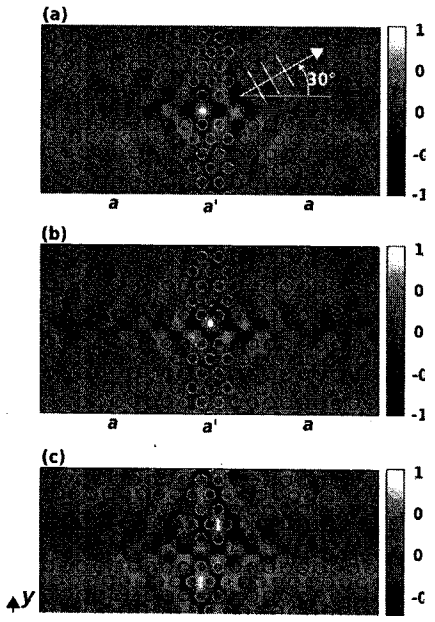

b. Multi-moded cavities

Much of the work on room temperature CW photonic crystal lasers involved lasers that were slightly larger than single defect photonic crystal lasers and therefore supported multiple modes. Significant work was done in this program to understand the mode structure and lasing behavior of these devices. The resonant frequencies and the quality factors of defect modes in a 19 missing-hole suspended-membrane photonic-crystal microcavity were calculated with 3-D FDTD and Pade's approximation. Good agreement was obtained between the calculated and the measured resonant frequencies. The resonant modes were classified by the irreducible representations of the C6v point group. The free-space far-field radiation patterns were calculated using a vector Green's function and the results compared favorably with polarization-resolved measurements. Although this work often focused on a particular 19-missing-hole triangular-lattice photonic-crystal

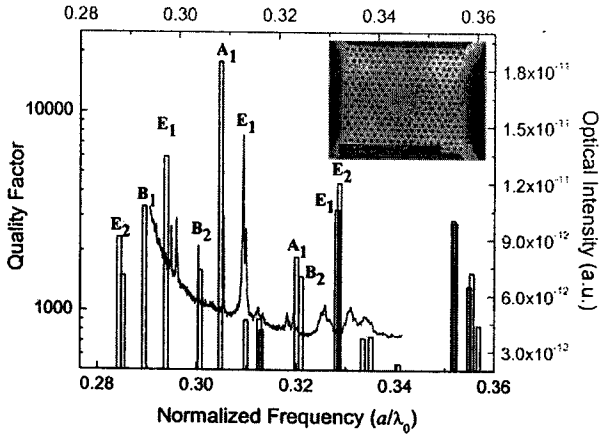

Fig. 1. Calculated resonance-mode frequencies and their quality factors for a suspended membrane 19-missing-hole photonic-crystal defect cavity (bars) with a membrane thickness of d/a =0.45 and hole radii of r/a=0.33 except the inner holes around the defect, which have slightly smaller r/a=0.3. It is compared with the measured photoluminescent spectrum of a cavity with similar dimensions (curve). The left and bottom axes are for the calculation, whereas the right and top axes are for the measurement curve. The difference of frequency is within 0.0035 in normalized scale, or ~16 nm in free-space wavelength. Resonance modes with a quality factor over 1000 in the material gain region are also labeled with their corresponding irreducible representation in the C_{6v} point symmetry group. The inset shows the top view of the cavity.

cavity, the method devloped here can be generally applied to the analysis of other multimode photonic-crystal microcavities. Even though the group theory was used to identify modes calculated from FDTD, it can also be applied in reverse. Enforcement of the symmetry properties of an irreducible representation during the numerical simulation restricts the resonant modes only to those satisfying the symmetry condition, thus allowing a wider numerical filter to be employed as the spacing between modes is generally increased, and therefore accelerating the convergence to the mode of interest.

Edge-emission and high output power in heterostructure lasers

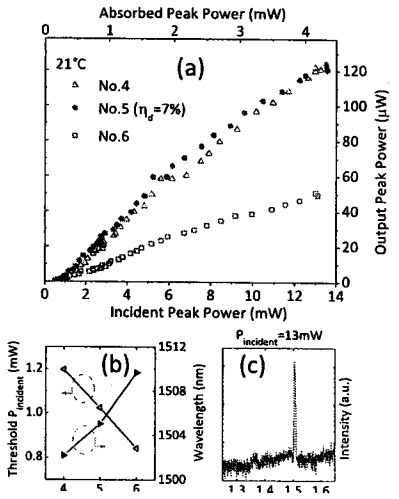

Shown at left is some recent data showing peak output power from a photonic crystal heterostructure laser. This was the highest output power yet demonstrated by about an order of magnitude at the time of the demonstration. The cavity volume in these devices is still on the order of $(\lambda/n)^3$. In addition, we also demonstrated a photonic crystal heterostructure laser in which the photonic crystal mirrors were no longer absorbing at the lasing transition energy because they had been disordered through an ion implantation step. This work resulted in an increase in the slope efficiency by more than a factor of two and a reduction in the threshold pump condition by about 40%. This should enable even higher output powers from these lasers in the future.

Room temperature CW operation on sapphire, Far-Field Design and Characterization, and Experimental Effort to Understand Cavity Loss

During the early part of this program effort was focused on three goals: developing photonic crystal lasers that could be optically pumped at room temperature under continuous wave conditions, developing photonic crystal lasers that could be electrically pumped, and better understanding the mode structure of multi-moded photonic crystal laser cavities. Optically-pumped photonic crystal lasers operating continuous wave at room temperature was achieved by bonding an active InGaAsP semiconductor membrane to a sapphire substrate and then fabricating the photonic crystal devices into the semiconductor membrane. These were the smallest, by an order of magnitude or so, photonic crystal lasers to operate at room temperature at the time. This work subsequently enabled a great deal of work in understanding and characterizing microcavity lasers dynamics and far-field radiation patterns. In addition, placing these devices on a substrate is still part of the research strategy with the goal of operating these devices directly on a semiconductor substrate. In order to achieve this, the optical loss into the substrate radiation modes must be understood and controlled. We continue to make progress in this direction.

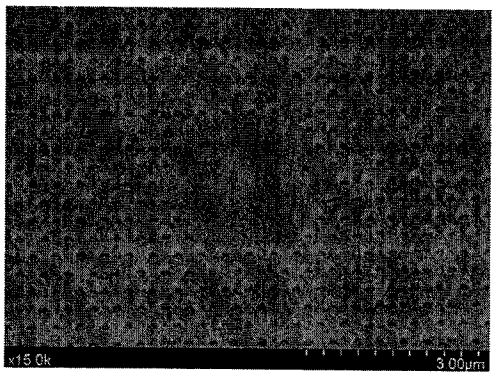

FIG. 1. Scanning electron microscope (SEM) image of a sapphire-bonded photonic crystal laser cavity from a 30° angle view. The lattice constant of the cavity is 400 nm.

The demonstration of photonic crystal lasers on sapphire substrates capable of optically-pumped room temperature CW operation opened up our ability to explore the far-field radiation patterns and later the microcavity laser dynamics of these devices. The far-field radiation patterns were theoretically modeled with a FDTD code with dyadic Green's functions incorporated into the analysis. Our FDTD code was written by my student Wan Kuang. We were able to predict the far-field radiation pattern of our lasers based on the lasing wavelength and our FDTD model for the near field and show that this was in excellent agreement with the experimentally measured far-field radiation patterns. We also worked to experimentally characterize the optical loss in these laser cavities on sapphire. We did this by fabricating an array of these lasers in which the central cavity geometry was constant across the array but the number of photonic crystal periods in the mirror varied across the array. This approach is somewhat analogous to measuring the optical loss in a Fabry-Perot edge-emitting laser by measuring the threshold behavior as a function of cavity length. By varying the mirror loss in the photonic crystal lasers by varying the number of photonic crystal layers cladding the cavity we obtained the threshold pump power variation with mirror loss. Then by converting the threshold pump

power to an effective threshold current density we could obtain a threshold gain as a function of mirror loss. From here, we converted the threshold gain to a cavity quality factor. The resulting optical loss extracted from the experimental data agreed with the calculated optical loss obtained from a FDTD simulation to better than 10%. The difference was attributed to absorption in the unpumped quantum well that was not included in the model. The modal properties of multi-moded devices were analyzed using

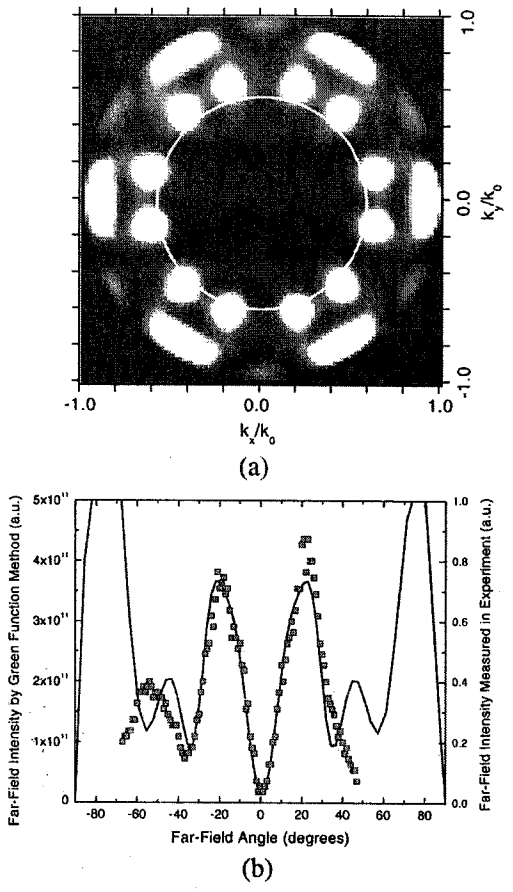

Fig. 4. (a) Calculated far-field intensity plotted as a function of its wave vector's projection on the k_x-k_y plane. (b) The experimental (squares) and theoretical (solid line) far-field radiation collected through the sapphire substrate in the k_y-k_z plane with variable polar angle.

Small-signal modulation response

The study of the modal structure of the CW photonic crystal lasers developed under this program is briefly summarized above. This study allowed us to demonstrate a single mode (nearly 30dB SMSR) CW photonic crystal laser that was optically pumped. This single mode CW performance allowed us to begin an effort that is still yielding results, namely an investigation into the small-signal modulation response as well as the laser linewidth. Another way to phrase this is that we began an investigation that asked the question "How small can a semiconductor laser be scaled and still be useful as a high-bandwidth signal transducer?" As the laser volume shrinks, several disadvantageous effects happen: the linewidth is expected to broaden (the linewidth is proportional to the average spontaneous emission rate into the lasing mode), amplitude fluctuations should

increase in significance as the photon number in the cavity shrinks, and there is a tradeoff in the cavity Q and the intensity inside the cavity that affects the threshold condition and the expected output power. In other words at high Q values the intensity inside the cavity is large enough to begin saturating the gain. To work in a linear gain regime, the Q must be kept to more moderate values (~1-2K for the cavity volumes that are typical in our work). This lower Q value increases the threshold pump power required but also, assuming the losses are output coupling losses, allows for more output power. In addition, a simple model for operating in the neighborhood of 10GHz suggests that laser output powers on the order of 100 microwatts are going to be necessary to achieve high enough signal-to-noise ratios to operate in the BER neighborhood of 10-9 or greater. \ This design strategy was also subject to the constraint that the device geometry be suitable for eventual electrical pumping. These early studies of the small-signal modulation response yielded demonstrations of -3dB bandwidths of just under 10GHz. Small-signal modulation response measured from a photonic crystal laser built under this program is shown above. We also observed that the behavior of the damping as a function of the bias point behaved consistently with the standard rate equation model for the modulation of semiconductor lasers. As these studies progressed, we accumulated data suggesting a significant gain compression term for these devices. We also characterizied the linewidth of the laser above threshold. This was the beginning of an effort to characterize the spontaneous emission rate into the lasing mode through the linewidth parameter.

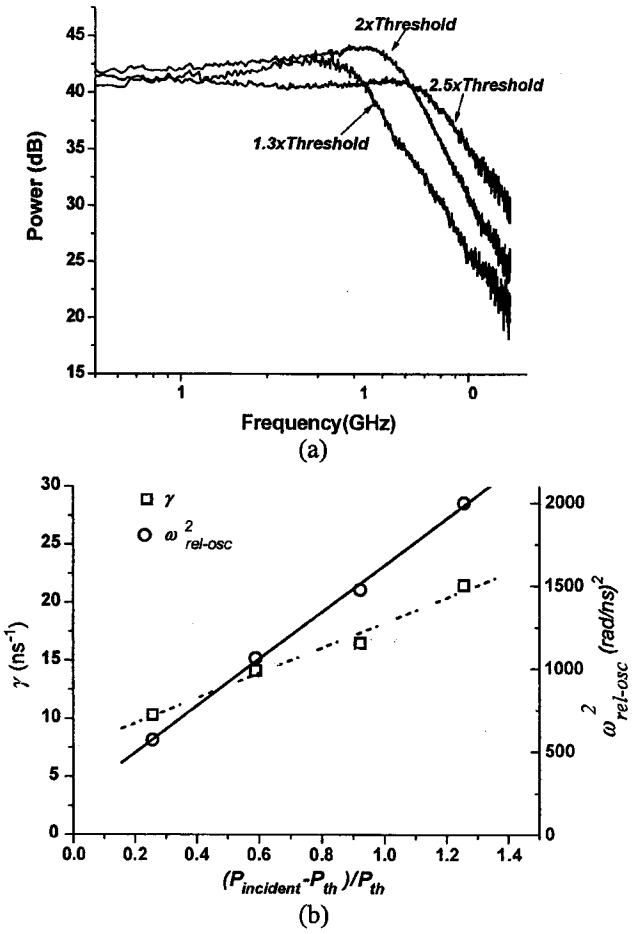

Fig. 4. (a) Small-signal modulation response of a 3.2-μm diameter cavity (D_4) at different bias levels. (b) Relaxation oscillation frequency squared ($\omega^2_{\mathrm{rel-osc}}$) and damping ($\gamma$) behavior versus the incident power for D_4 cavity.

Lasers with quantum dot active regions

In addition, work done on photonic crystal lasers incorporating quantum dot active regions is included in this report. While this work was not directly supported by this program, it relied heavily on results obtained in this program and students supported by this program worked closely with Tian Yang who was the student responsible for the quantum dot work in my group. The micrographs below show microdisk and photonic crystal laser cavities with quantum dot active regions.

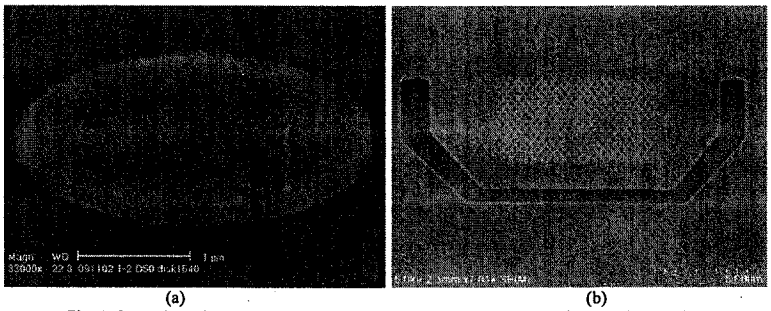

(a) (b)

Fig. 1. Secondary electron micrographs of (a) microdisk [3]; (b) photonic crystal L3 cavity.

Waveguides and Passive Components

Efficient fiber coupling

We first proposed and analyzed a highly efficient method of coupling light from optical fibers to two-dimensional photonic crystal waveguides. Efficient coupling is achieved by positioning of a tapered fiber parallel to the linear defect, where the photonic crystal's cladding functions as a grating coupler and provides field confinement as well. Numerical simulations indicate that better than 90% transmission is possible with a full width at half-magnitude bandwidth of 12 nm. It was shown that one can increase the bandwidth by increasing the field overlap between the two waveguides.

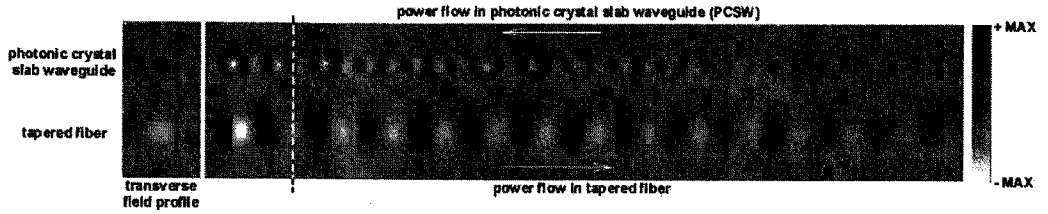

Fig. 2. Magnetic-field magnitude profile, showing contradirectional coupling of energy from a tapered fiber to a PCSW, calculated by 3-D FDTD. The power flowing from left to right inside the tapered fiber gets significantly weaker by coupling energy to the photonic crystal waveguide. Meanwhile, the power flowing from right to left in the photonic crystal waveguide becomes stronger with the interaction.

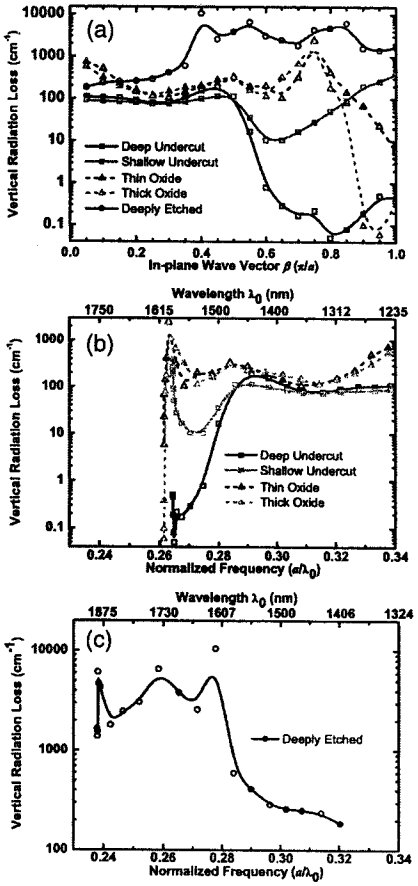

Fig. 2. Out-of-plane radiation loss as a function of (a) the in-plane wave vector β and (b), (c) the normalized frequency for the photonic-crystal defect slab waveguides modeled in this work. The lattice constant a = 450 nm for the deeply etched waveguide and 420 nm for the rest

Reducing the out-of-plane loss

A fully three-dimensional finite-difference time domain numerical model was developed and presented for calculating the out-of-plane radiation loss in photonic-crystal slabwaveguides. The propagation loss of a single-line defect waveguide in triangular-lattice photonic crystals was calculated for suspended-membrane, oxidized- lower-cladding, and deeply etched structures. The results, shown at left, show that low-loss waveguides were achievable for sufficiently suspended membranes and oxidized-lower-cladding structures.

Two-dimensional photonic crystal linear

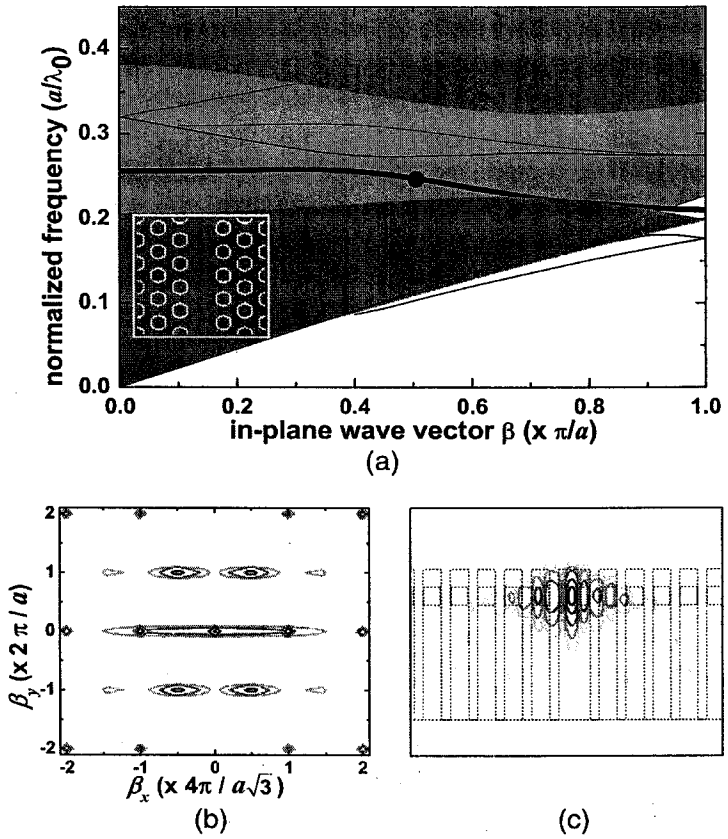

Fig. 2. (a) Photonic band diagram for a type B single-line photonic crystal defect waveguide in a reduced Brillouin zone scheme. The defect mode analyzed for out-of-plane radiation loss is marked by the thick curve. (b) Fourier transform of the in-plane waveguide dielectric distribution. (c) $H_z{}^2$ cross section for the defect waveguide mode at $\beta_y = 0.5\pi/a$. The dotted lines outline the waveguide dielectric distribution. The field contour has one additional gray level compared with 1(e) to identify the radiation path.

defect waveguides on semiconductor substrates were studied. It was predicted that the out-of-plane radiation loss could be reduced by more than one order of magnitude by shifting one side of the photonic crystal cladding by one-half period with respect to the other along the propagation direction. This idea became an important component of the strategy to demonstrate photonic crystal devices on semiconductor substrate without the need to form suspended membranes.

Demonstration of a Mach-Zehnder interferometer

The experimental work in this area focused on demonstrating Mach-Zehnder interferometers. A variety of interferometers were demonstrated ranging from devices that had equal length arms to devices with varying asymmetries in the path lengths of the two arms. This was done because we were looking for an oscillation in the transmitted intensity with wavelength. For asymmetric Mach-Zehnders, the output intensity should oscillate as the wavelength is varied because the total accumulated phase in each arm is a function of wavelength. This was done so that we were convinced that the transmitted

beam contained an optical signal from each arm in the devices. In other words, this oscillation was a signal that each of the y-branches and all of the bends were working because only if this was true would we see an oscillation in the intensity that resulted fro

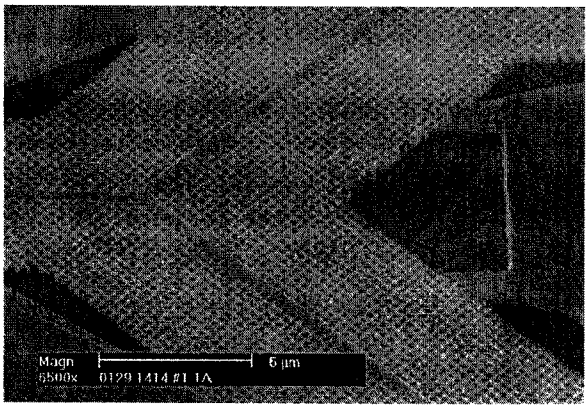

FIG. 2. SEM micrograph showing the part of the Mach–Zehnder structure near one of the Y branches.

m a summing of the two arms. The spectral period of these devices also allowed us to infer information about the group velocity in the photonic crystal waveguides. This was among the first demonstrations in passive photonic crystal devices to combine bends and branches in a working component.

An effort in the demonstration of photonic crystal directional couplers, fabricated in the SOI material system was also undertaken during the course of this program. This work built on the significant modeling effort during the course of this program. We also demonstrated that these devices could be switched by optically illuminating the junction region.

The finite-element method including simulated annealing algorithm was adopted for the analysis and optimization of photonic crystal waveguiding structures. The dispersion relations of photonic crystal waveguides were found by solution of an eigenvalue equation. The waveguide structures including bends and branches were analyzed by means of a scattering formulation. The symmetry of the structure was exploited to classify the modes as well as to reduce the computational resources needed. Based on the transmission spectra of a waveguide's bends and branches, a branch was optimized using the simulated annealing method. We found qualitative agreement between these predictions and experminental data.

Experimental determination of the optical bend loss in a photonic crystal waveguide bend or junction

The work on photonic crystal waveguides in this time period resulted in an experimental measurement of the optical transmission loss through a photonic crystal waveguide bend. The approach was to form consecutive bends in a photonic crystal waveguide and vary the distance between the two bends from one device to the next. Any reflection at the bends would result in the formation of a Fabry-Perot interferometer between the two

bends. This interferometric effect would manifest itself in the usual oscillation in the transmitted spectrum as a function of wavelength. By varying the length of the waveguide between the two bends we could look for an oscillation signature in which the period of the oscillation varied inversely with the separation between the bends. Once this signature was identified, we could use a Hakke-Paoli approach to characterize the reflectivities of the bends. Once this was accomplished we found excellent agreement between the measured bend reflectivity and the reflectivity that had been calculated earlier using a finite element approach.

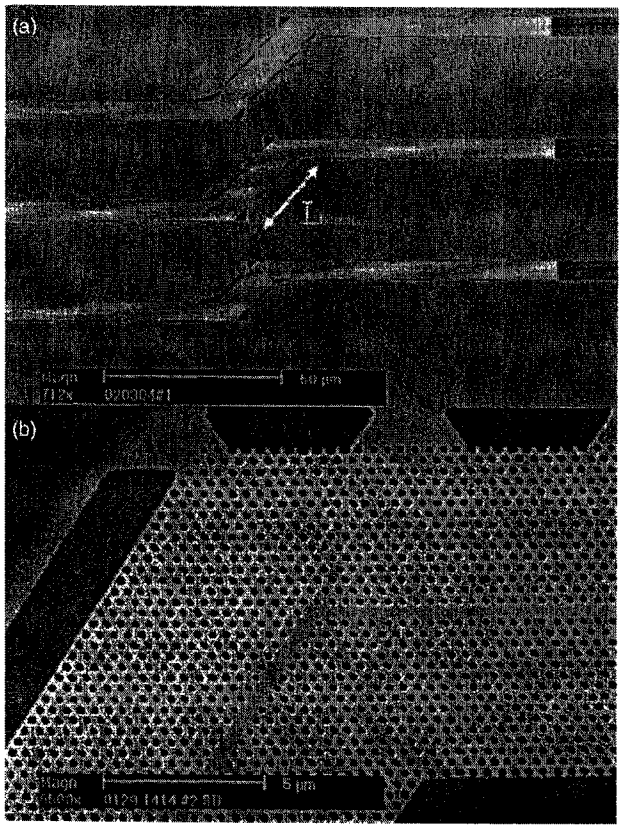

FIG. 1. a Scanning electron micrograph showing parts of three doubly bent PCWGs with the different waveguide lengths between the bends. b A magnified view of a 60° waveguide bend.

Recent Progress: Photonic Crystal Lasers

USC Viterbi School of Engineering

We have obtained 100 μW of peak output power from a photonic crystal laser. This is the largest reported output power to date.

This was obtained from an edge-emitting photonic crystal heterostructure cavity. The mode volume of this cavity is just over one λ^3.

Our target fiber-coupled output power is 100 μW. We believe that this can be achieved in the near future.

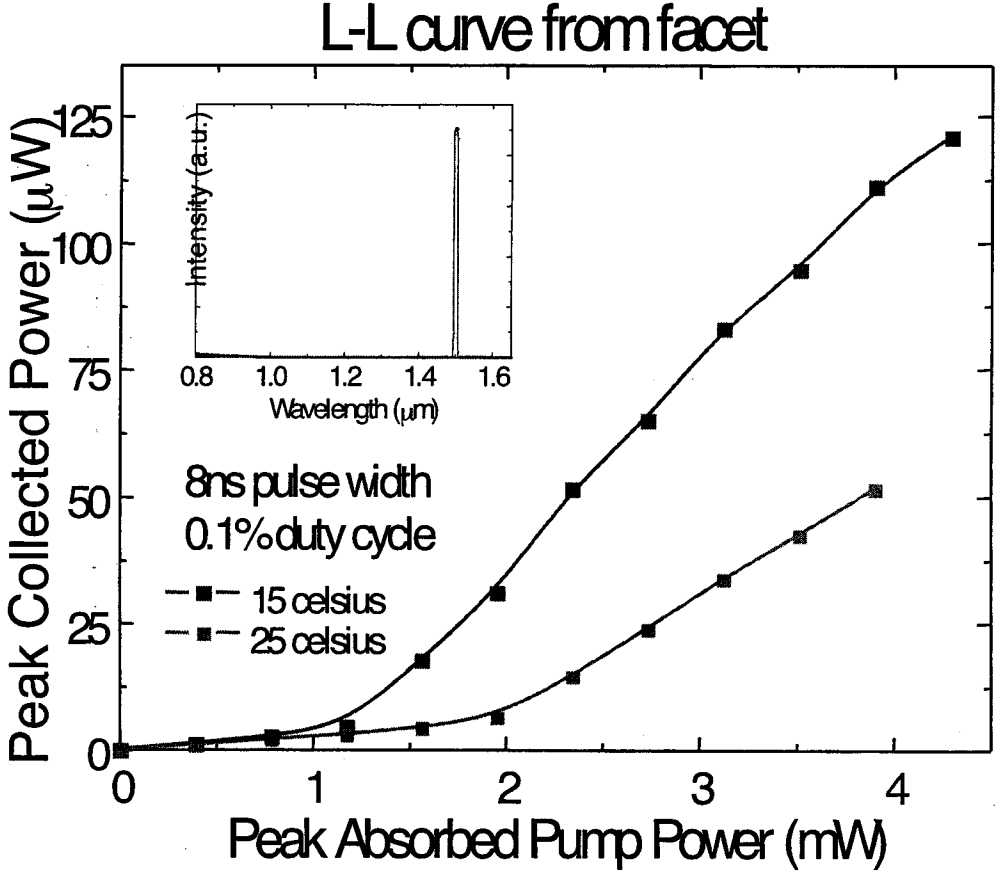

We also believe that this device can be operated on a substrate that will allow room temperature CW operation. The belief is based on FDTD models that predict quality factors of these cavities on a substrate that are consistent with our existing CW lasers.

USC

Recent Progress: Photonic Crystal Lasers

USC Viterbi School of Engineering

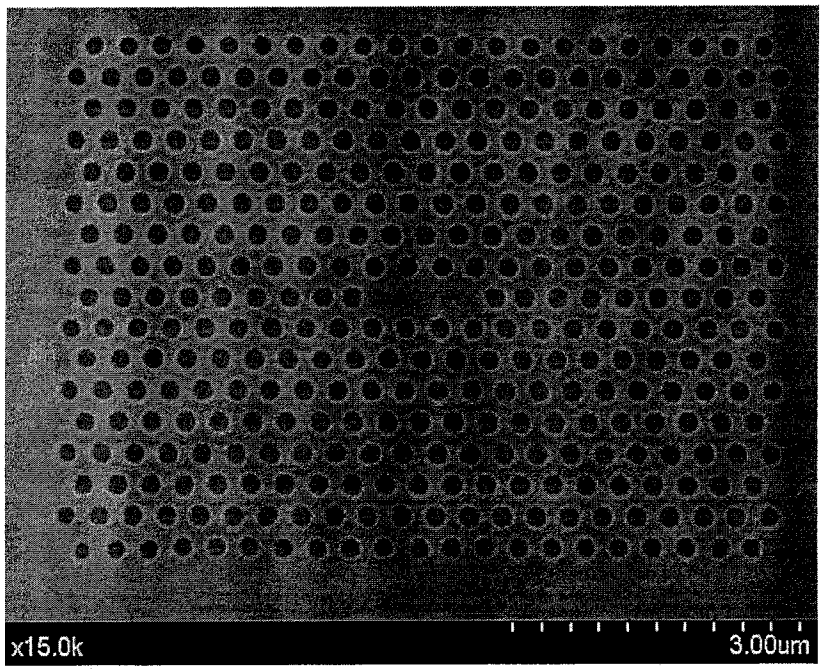

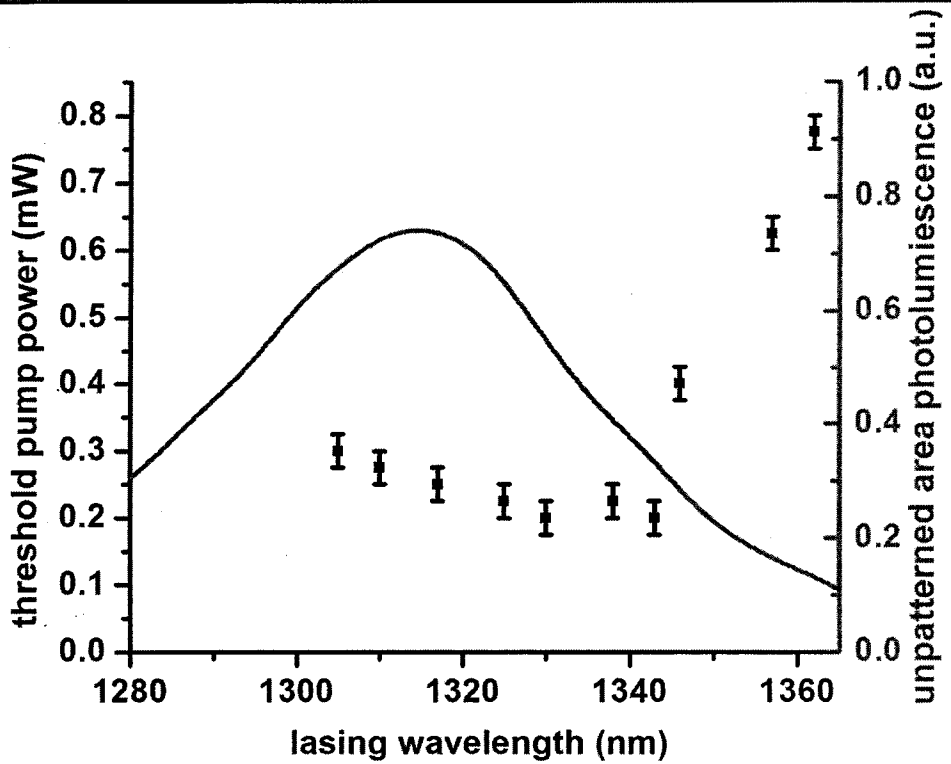

We have made progress in obtaining very low threshold lasing in photonic crystal cavities with quantum dot active regions and have obtained lasing with only a few dots participating

- Our lowest threshold value to date (9 μW absorbed)
- 5-6 dots are estimated to be participating in the lasing at the longest wavelengths (homogeneous broadening ~ 5 nm)

USC

Recent Progress: Passive Photonic Crystal Components

USC Viterbi School of Engineering

- We have improved our SOI photonic crystal waveguides.
- We have observed 1.25 dB/mm of optical loss.
- We have observed group indices as large as 19.

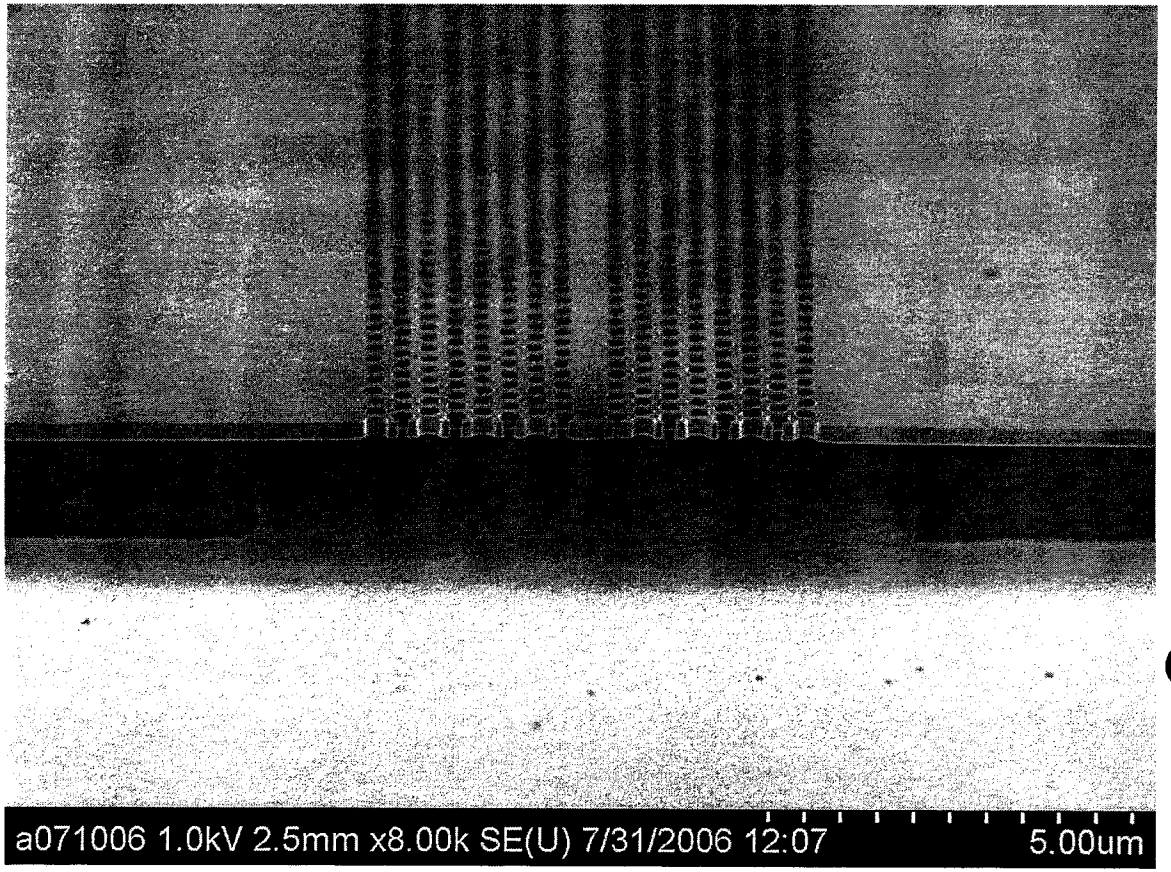

USC

Recent Progress Passive Photonic Crystal Components

USC Viterbi School of Engineering

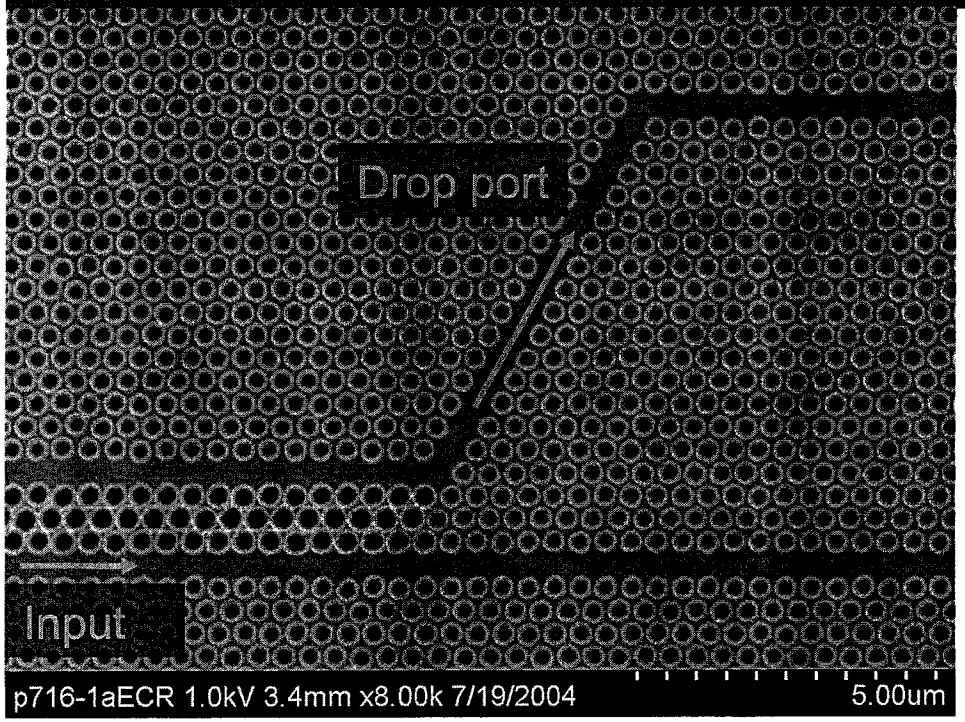

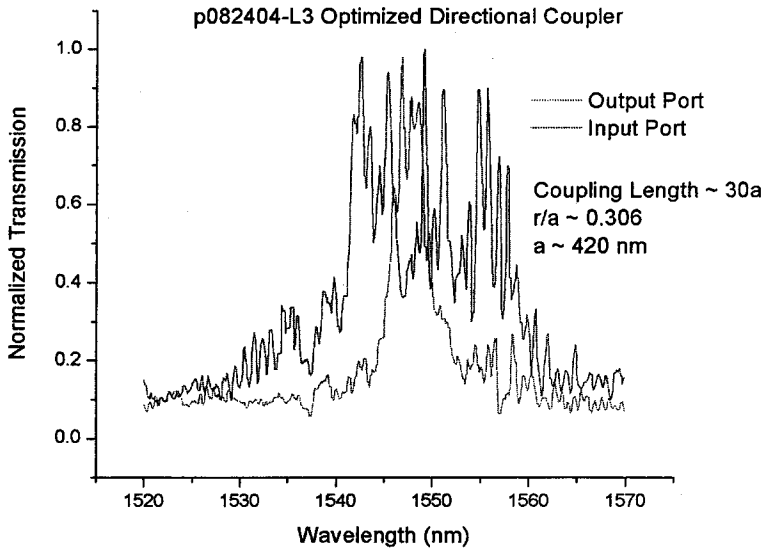

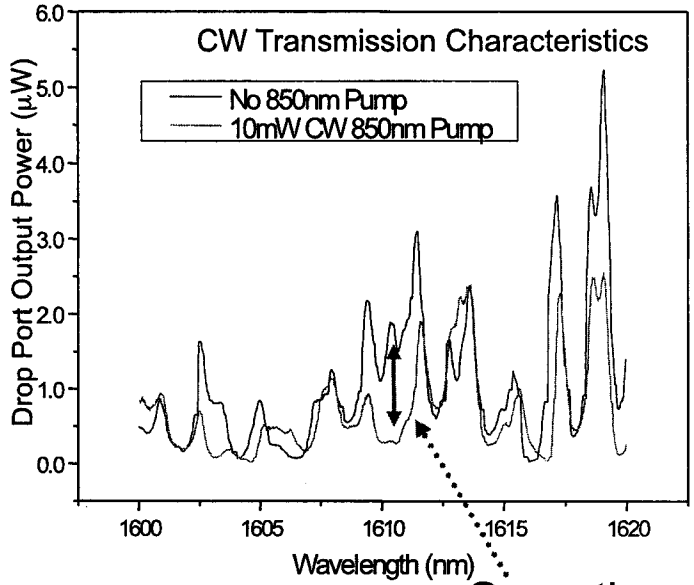

Directional couplers are formed in SOI by two waveguides with 3 rows of holes between them.

We have observed extinction ratios (Drop Port / Input Port) in excess of 10dB

We have demonstrated switching in this device with 10 mW of optical power incident on the coupling region.

USC

Key accomplishment for the program to-date

USC Viterbi School of Engineering

- Demonstrated Lasing in Cavity Bonded to SOI

  Room temperature, optically pumped operation from InGaAsP membrane on SOI with 1 micron oxide thickness.

- Demonstrated Room Temperature CW Lasing in Cavity on Sapphire

  Smallest such laser by about a factor of 10
  This has led to characterization of the far-field and laser dynamics
  25dB SMSR, and analog modulation >12 GHz demonstrated.

- Demonstrated Lasing in Cavity with Quantum Dot Active Region (in collaboration with Dennis Deppe)

  ~9 microW absorbed power at threshold, lasing at 1340 nm

  5 layers of InAs quantum dots each with density of $2x10^{10}$ cm^{-2}

- Electrically Injected Resonances (cavity lases under optical pumping)

  series resisitance reduced in recent samples

- Prediction and Design of Low-Loss Waveguides on SOI W/O Suspended Membrane On a high index substrate, the out-of-plane radiation loss is reduced by about two orders of magnitude in type-B waveguides due to destructive interference in the radiation fields. Minimum predicted loss is ~ 5 cm^{-1}.

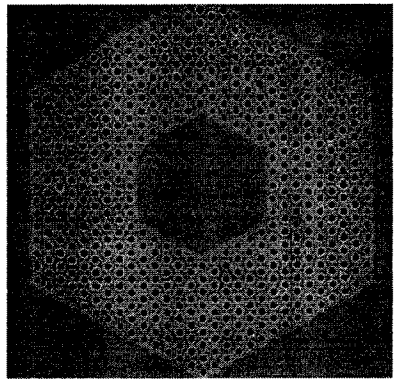

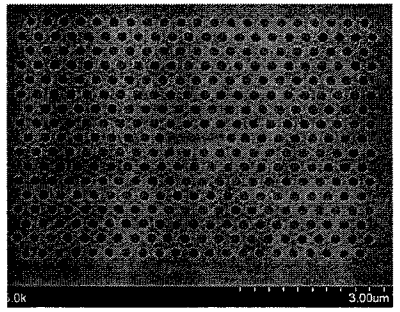

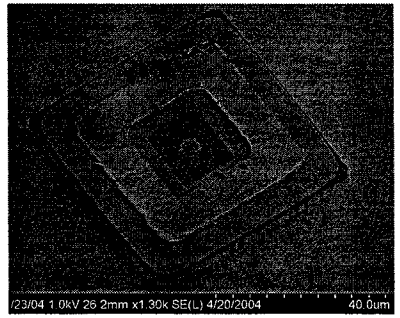

USC

Key accomplishment for the program to-date

USC Viterbi School of Engineering

- Demonstrated Lasing in Photonic Crystal Heterostructure Cavity with Quantum Dot Active Region (in collaboration with Dennis Deppe)
  this cavity ideal for high output power collection efficiency

- Demonstrated Lasing in Type-B Heterostructure Laser Cavities

  This design allows photonic crystal lasers to be places on high index substrates making it a very attractive candidate for electrically-pumped designs.

- Demonstrated Optimized Photonic Crystal Y-Branches and Directional Couplers in SOI

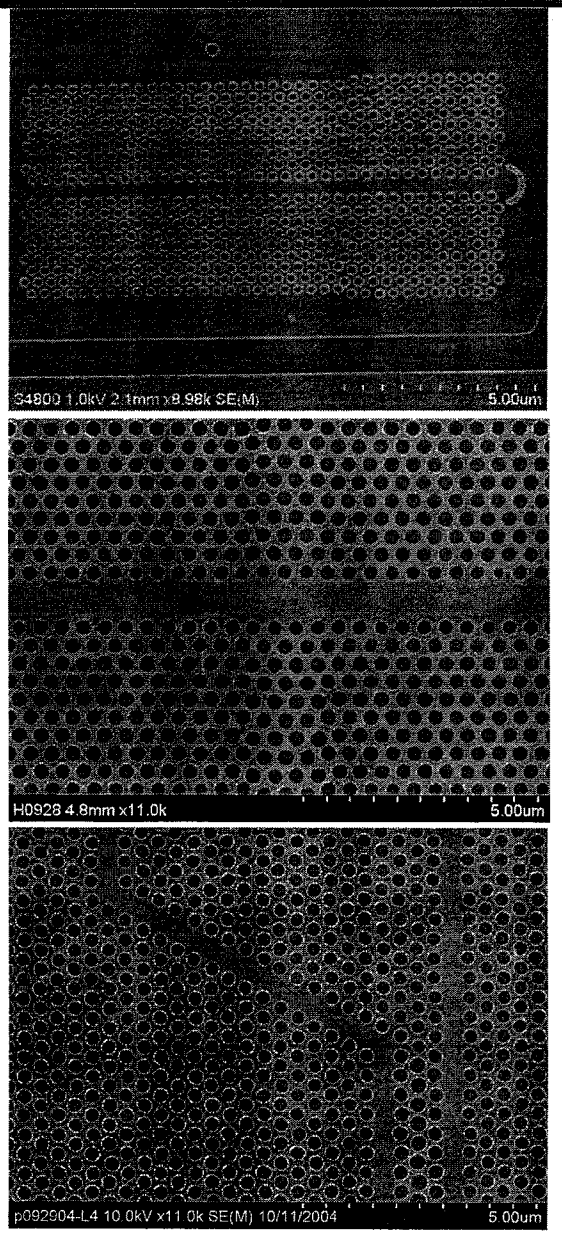

USC

Key accomplishment for the program to-date

USC Viterbi School of Engineering

- Proposed and demonstrated low insertion loss evanescent coupling from fiber to photonic crystal waveguide

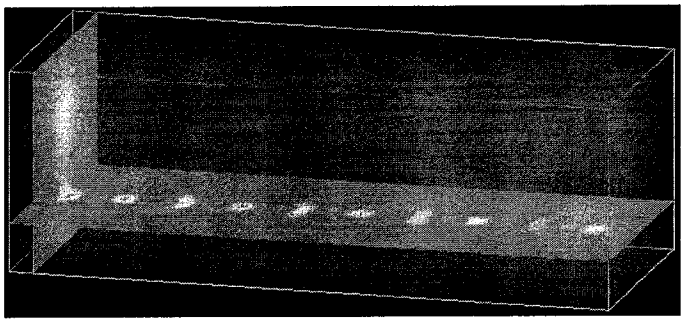

- Demonstrated photonic crystal Mach-Zehnder Interferometers

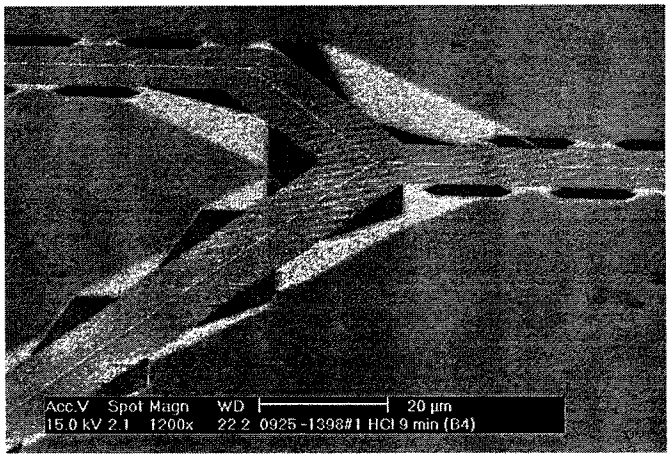

- Demonstrated Room temperature CW operation in 6.9 µm diameter microdisks with Al_xO_y layer below the disk for heat dissipation
(in collaboration with Dennis Deppe)

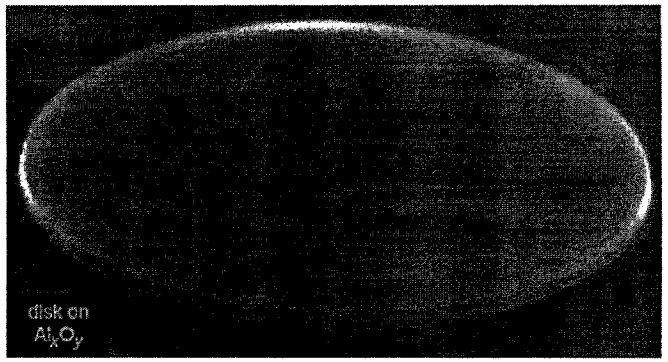

USC

Detail how your work has demonstrated the program goals

USC Viterbi School of Engineering

- We have demonstrated modulated lasers, waveguiding, and switching in photonic crystal technology

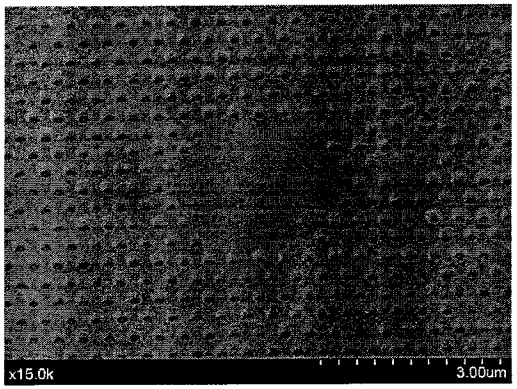

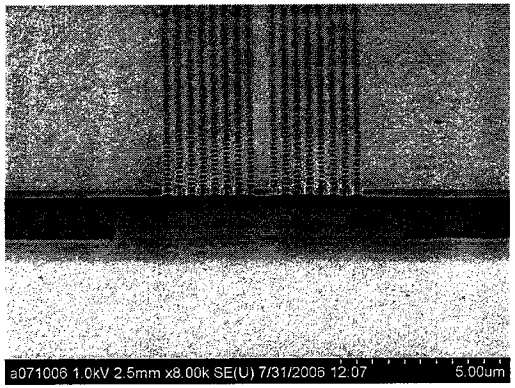

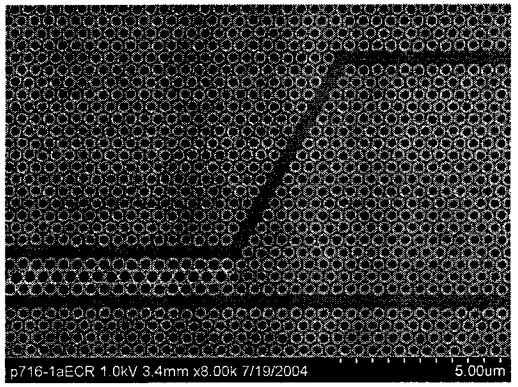

- We have demonstrated small-signal modulation in lasers with a 3 dB frequency of 12 GHz.

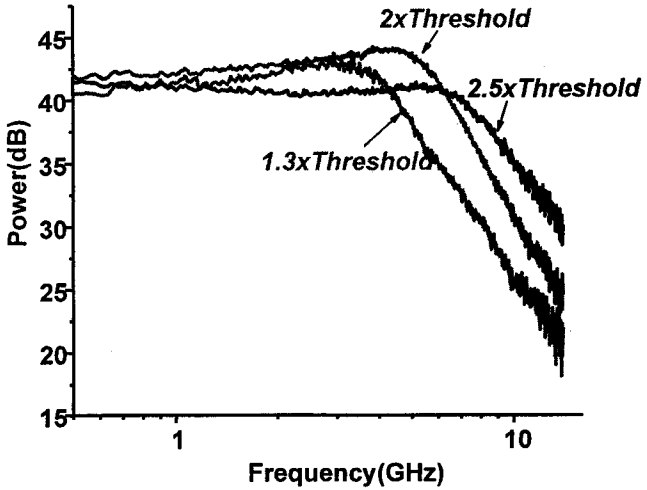

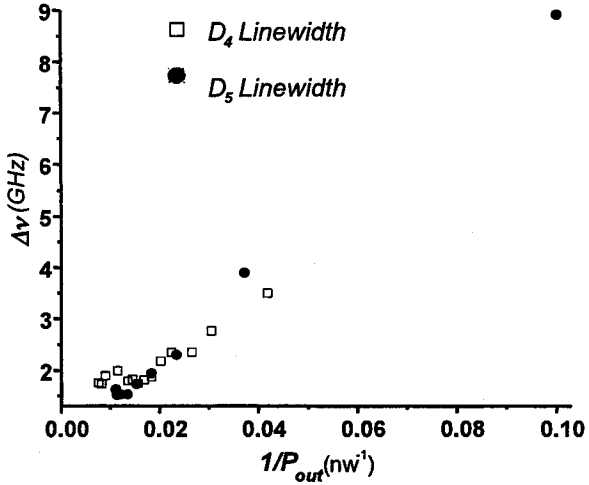

USC